FINAL REPORT

Title: Assessing the effects of pile burning-induced soil heating in Alaska's boreal forest

JFSP PROJECT ID: 24-1-01-7

December 2025

Michelle C. Mack, PhD
Northern Arizona University

Matthew Behrens, MS
Northern Arizona University

TABLE OF CONTENTS

LIST OF TABLES

LIST OF FIGURES

LIST OF ABBREVIATIONS

NPS	United States National Park Service
DNPP	Denali National Park & Preserve
SOL	Soil Organic Layer
DBH	Diameter at Breast Hight
CWD	Coarse Woody Debris
TCP	Thermocouple Probe
GLMM	Generalized Linear Mixed Model

KEYWORDS

Alaska, Denali National Park & Preserve, boreal, fuel treatment, fuel reduction treatment, hand-thinned fuel treatment, soil heating, pile burning, fire, burn depth, carbon emissions, ash, charcoal, soil nutrients, soil

ACKNOWLEDGEMENTS

This project was funded by the Joint Fire Science Program, the National Park Service (Cooperative Agreement P24AC01648), the Center for Ecosystem Science and Society, Office of the Vice President for Research at Northern Arizona University, the Brad McRae Fellowship, the Bonanza Creek Long-term Ecological Research Program (NSF DEB-2224776) and the Navigating the New Arctic Program (NSF OPP-2127284). We thank National Park Service Alaska Region collaborators and staff for their contributions and commitment to this work. We are grateful to Sarah Stehn, Jennifer Barnes, Kieth Mitchell, Matt Kohler, and both the fire suppression and fire ecology field crews of NPS Western Area Fire Management for their organizational support, expertise, and professionalism in bringing this work to life.

FIRE'S FOOTPRINT: UNDERSTANDING SOIL HEATING AND FIRE EFFECTS IN DENALI NATIONAL PARK & PRESERVE'S PRESCRIBED PILE BURNS

Abstract

Prescribed pile burning is increasingly used as a fuel-reduction treatment in boreal forests. However, the belowground thermal and biogeochemical effects of pile burning at high latitudes remain weakly quantified, and implementation occurs without empirical evidence to support practitioner decisions. Clear links between practitioner-controlled factors and soil outcomes are necessary to balance wildfire risk reduction with informed stewardship. We evaluated soil heating and first-order fire effects at hand-constructed piles in Denali National Park & Preserve. Treatments varied in season of burn, soil organic layer depth, and pile volume. We instrumented 59 piles with temperature sensors at multiple depths and lateral distances, and measured burn depth, belowground carbon and nitrogen loss at an additional 59 piles. We measured soil pH, and plant-available nutrients during the first post-burn growing season at 80 piles and 40 unburned control sites. We found that heating was shallow, confined to the pile footprint, and lower in Spring compared to Fall. Specifically, spring burns over frozen soils limited peak temperature, exposure time, and depth relative to fall burns over thawed soils. Soil organic layer depth buffered mineral soil heating. Larger piles modestly increased burn depth into the organic layer but did not broadly intensify heating. Changes in belowground carbon and nitrogen were driven primarily by pile volume and organic layer depth, and nitrogen generally declined. Burned soils became more alkaline and exhibited a short-term nutrient pulse. Together, these results show that season of burn and soil organic layer depth largely determine soil heating, and belowground carbon and nitrogen loss, giving practitioners actionable guidance for scheduling and siting pile burns that meet fuel-reduction goals in boreal forests and support landscape stewardship decision-making.

1. Objectives

The Graduate Research Innovation Award was used to supplement a master's thesis on the effects of pile burning on boreal forest soils at Denali National Park & Preserve. The award allows us to add the component of soil heating to our geochemical investigation of the first-order effects of pile burning to soils. The aim of this project was to quantify the impacts of pile burning to soils across a range of forest and soil types that are representative of the Alaska Range and Interior Alaska and to test how practitioner decisions alter the observed impacts. We addressed three objectives that guided the analysis. First, we quantified soil heating at time of burn to capture the magnitude, duration, and vertical penetration of heating. We expected fall burns and larger piles to generate greater heating, with stronger effects where pre-fire SOL depths were shallow. Second, we estimated pile burning impacts on soil C and N pools per unit area within pile burns to evaluate element addition or loss. We anticipated no seasonal effect on soil C and N pools but predicted greater net C and N losses with larger piles and with deeper SOL depths. Finally, we compared burned to unburned soils to assess plant-available nutrients and soil pH during the first growing season after burning to characterize impacts important for plant recovery within piles. We expected lower nutrient supply rates in fall than spring pile burns and higher pH in burned than unburned soils.

Together, these investigations provide a practitioner-relevant account of pile burning's first-order fire effects and supply actionable evidence for treatment design in Interior Alaska. This evidence enables calibration of prescriptions that lower wildfire risk, avoid unintended impacts such as erosion and permafrost thaw, and ensure rapid recovery of soils and vegetation towards a desired future state.

2. Background

Interior Alaska faces two converging pressures: a warming climate is driving larger, more frequent wildfires, and the wildland urban interface is expanding. This makes proactive fuel management essential to protect human lives and infrastructure (Duffy et al., 2005; Kasischke et al., 2010; Liang et al., 2022). Fuel reduction treatments, hereafter "fuel treatments," are used to reduce fire spread and protect at-risk areas by modifying fuel structure and continuity (Ott & Jandt, 2005). To implement a hand-thinned fuel break, crews use chainsaws and hand tools to remove whole trees, limbs, and debris, which is then stacked into piles and burned when conditions are favorable for preventing uncontrolled fire spread. As piles are combusted, substantial heat is generated , with cascading effects on plants, soil organisms, carbon (C) and nitrogen (N) pools, and nutrient dynamics (Mott et al., 2021). Given the growing prevalence of pile burning in Interior Alaska, practitioners require a refined understanding of its impact on soils to inform decisions that support treatment objectives and promote good land stewardship.

Key operational features of pile burning that could strongly influence soils include season of burn, pile volume, and depth of the SOL. Pile burning usually occurs in fall or spring, often with snow present. Second, fuels are stacked into compact piles that concentrate combustion within a small area and include tree stems and coarse woody debris (Busse et al., 2013). Empirical studies in the Pacific Southwest and British Columbia show that mineral soil temperatures under piles can exceed 700°C and remain elevated for days, indicating intense, localized heating that penetrates underlying soil (Busse et al., 2013; Smith et al., 2016; Switzer et al., 2012). Third, piles produce discrete burned patches with minimal spread beyond the footprint

and focus deposition of ash and charcoal to the soil (Busse et al., 2013; Switzer et al., 2012). Although these observations come from temperate systems, the intense, prolonged, and localized nature of pile combustion points to soil heating as an important mechanism for anticipating soil impacts in boreal settings.

The primary pathway by which pile burning affects soils is elevated temperature; concentrated combustion raises subsurface temperatures for hours or days (Mott et al., 2021). This matters because biologically and geochemically important processes begin at temperatures that are often exceeded beneath piles in other regions (700°C; Busse et al., 2013). For example, organismal tissue damage begins near 40°C and plant root mortality occurs between 48–65°C, with the severity of impacts increasing with both temperature and exposure duration (DeBano, 1998; Pingree & Kobziar, 2019; Ryan et al., 2012). At higher temperatures, key nutrient transformations occur, including ammonium volatilization at approximately ≥300°C and phosphorus mineralization at approximately ≥500°C (DeBano, 1998; Massman et al., 2010; Ryan et al., 2012), and these changes have been associated with post-burn increases in soil pH (Pereira et al., 2015; Switzer et al., 2012). Whether these temperature thresholds and exposure times are reached in Alaska's boreal soils, and thus whether the associated biological and biogeochemical impacts occur, ultimately depends on the soil context that governs heat transfer and residence time.

Findings from other ecosystems may not be generalizable to boreal systems due to their unique environmental conditions, including perennially frozen (permafrost) or seasonally frozen soils (Jorgenson et al., 2010), high soil water content (O'Donnell et al., 2009), and deep, spatially variable soil organic layers (SOL; Johnstone et al., 2010; Roland et al., 2013) that insulate the mineral soil from heating but may also be combusted when dried sufficiently (Santín et al., 2016). These conditions change how heat moves into the soil (DeBano, 1998; Massman et al., 2010). As a result, outcomes documented elsewhere may not predict mineral soil temperatures, crossings of key thresholds, or changes in C and N pools, nutrient availability, and pH under pile burns in boreal forests. Despite the growing application of pile burning in Alaska, quantitative evidence linking these unique environmental conditions to soil heating and its impacts is limited. Thus, practitioner-controllable choices in pile burning design and implementation present a means to shape soil heating and the near-term nutrient and soil impacts it drives.

Three practitioner-controlled variables are likely to structure the soil heat pulse of pile burning in boreal settings. These are the season of burn, the depth of the SOL where piles are constructed, and pile volume. In high latitude climates, the season of burn largely determines whether soils are frozen or thawed. When soils are seasonally or perennially frozen, additional energy is required for phase change of water and ice, which can dampen and delay subsurface heating relative to thawed soils (Hinkel & Outcalt, 1994; Outcalt et al., 1990). The SOL moderates how heat reaches the mineral soil. Greater SOL depth insulates the mineral soil and reduces heating. When sufficiently dried, it can combust and contribute further heating that drives deeper penetration. Because SOL depth varies within sites, choosing where to place piles can influence subsurface temperature profiles. Pile volume likely governs total heat release, with larger fuels tending to sustain higher temperatures for longer periods (Busse et al., 2013). Together, these practitioner controllable elements frame testable questions about how to guide the magnitude, duration, and depth of soil heating and the near-term soil impacts in support of good stewardship and informed prescription design.

We examined how season of burn, pile volume, and pre-fire SOL depth shape soil heating, combustion, and materials addition when pile burning in Denali National Park & Preserve, Alaska. In collaboration with National Park Service (NPS) Fire Management, we established six fuel treatments across stands that varied in structure and SOL depth. Thinning and pile construction followed NPS standard operating procedures. Piles were stratified by volume and randomly assigned to fall or spring burns to isolate seasonal and pile volume effects. We instrumented piles and adjacent soils to capture the burn period heat pulse, linking practitioner choices to observed soil responses.

3. Materials and Methods

Site Description and Study Design

We conducted this study in the front country of Denali National Park & Preserve (DNPP; 63°43' N, 148°55' W). The climate is subarctic continental with long cold winters and short warm summers (Clark & Duffy, 2006). Based on 100 years of climate records at Park Headquarters, annual precipitation averages 40.1 ± 0.15 cm (mean ± standard error) and mean monthly air temperature ranges from −16.5 ± 0.9°C in January to 13.2 ± 0.2°C in July (National Park Service, 2022). Mean annual air temperature is -2.1 ± 0.2°C (National Park Service, 2022). Soils are Typic Haplocryods and Typic Historthels (Clark & Duffy, 2006). Tree species in the study area include white spruce (*Picea glauca* (Moench) Voss), black spruce (*Picea mariana* (Mill.) BSP), and trembling aspen (*Populus tremuloides* Michx.).

During summer 2023 and 2024, federal crews implemented 10.52 ha of fuel treatments to reduce wildfire risk to park infrastructure and increase options for egress. Crews used chainsaws and hand tools to remove fuels following a prescription to thin trees to 10 ft stem spacing (1,077 stems ha^{-1}) and to remove limbs up to 6 ft high. Resulting woody debris was piled in place by stacking cut wood and branches lengthwise to form half-cylinder piles. Under the burn prescription, piles were ignited when at least 1 inch of snow covered the ground and eye-level wind speed was less than 10 mph. Crews lit piles with drip torches and minimally tended them ("chunked") in accordance with NPS operating procedures and burn plans. Burn scheduling was conducted by NPS Fire Management, beginning to burn piles at the earliest permissible window. Sites A and E were prepared in summer 2023, and sites B, C, D, and F in summer 2024 (Figure 1). All sites were burned in fall 2024, creating a single shared fall window. Spring burns bracketed that fall window, with twenty piles in spring 2024 (ten at A and E) and forty in spring 2025 (ten each at B, C, D, and F). This staggered schedule reflects operational constraints while preserving the seasonal contrast. In these recently implemented fuel treatments, we established six sites (hereafter sites A-F; 0.5–1.75 ha each) that represent a range of forest composition and soil organic layer depths characteristic of DNPP lower elevation landscapes (Supplementary Figure 1; Roland et al., 2013). These low to mid elevation (500–640 m) sites are dominated by mixed spruce and broadleaf deciduous forests. Two of six sites (E & F) contain discontinuous permafrost common in poorly drained upland areas of the park.

After thinning was completed, we determined the number and linear dimensions of all piles. For each pile, we recorded two height (h) measurements and measured each side's width (w) or length (l), yielding two measures of each. We calculated the volume of each pile as a half cylinder using mean dimensions ($V = (\pi \times w \times l \times h)/4$; m^3). Within each site, we stratified piles

into five volume classes based on the range of measured piles using the geometric-interval classification in ArcGIS Pro (Esri, Redlands, CA). Pile volume classes differed between sites in order to capture the full range of pile volumes resulting from typical operations. At each site, we randomly selected four piles from each volume class, yielding 20 piles per site and 120 in total. We randomly assigned these piles to burn season (fall or spring) within each site. Within each volume class and season, we then randomly assigned the soil temperature sensor treatment (temperature sensors installed vs. none). This nested design yielded five instrumented piles per site in fall and five in spring for soil heating, plus five additional piles per site in each season for combustion and for C and N accumulation and loss.

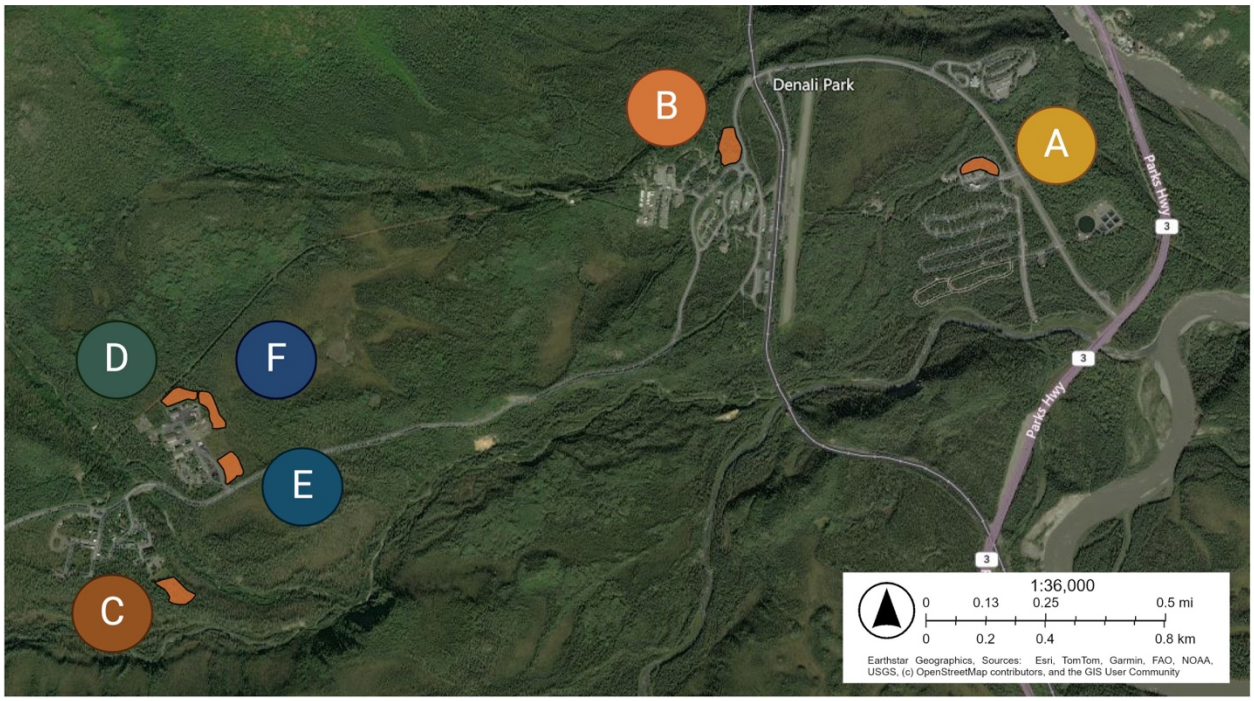

Figure 1. Map of six sites contained within the study. Sites are located within the Visitor Service Area of Denali National Park & Preserve.

For each selected pile, we visually assessed pile composition by wood species. For each size class (1-10hr, 100hr, 1000hr, boles >15cm diameter; Brown, 1974) within each species, we recorded decay status (standing when cut or dead and down) by visually estimating the proportion of pile volume. We also established a circular plot with a 6-m radius from the pile center and counted remaining tree stems. For all trees taller than 1.37 m, we recorded diameter at breast height (DBH), distance from plot center, species, and whether the tree was alive or dead. We computed the basal area for individual trees as $BA = (\pi/4) \times DBH^2$, basal area per hectare, and tree density per hectare by species for each pile.

Soil Heating Field Methods

We investigated vertical and horizontal soil heating in 59 piles; one pile was lost because it was unintentionally burned. Each pile was instrumented with Type-K thermocouple probes (TCPs) rated for >1000°C (ARI Industries, Addison, IL) and iButtons attached to wooden stakes (Brady et al., 2022; Supplementary Methods). To measure horizontal heating, we aligned a

sensor transect with the long axis of each pile. The day before burning, we partially deconstructed each pile to expose the soil up to the pile center, installed TCPs at the mineral soil surface, and then reconstructed the pile. Thermocouples were placed at 0, 100, 200, and 300 cm from the pile center along the transect. Pile edge was defined as one half of the mean of the two measured pile lengths. We buried TCP wire leads along the mineral–organic interface to four-channel data loggers housed in waterproof cases (Onset Computer Corporation, Pocasset, MA). Temperature was recorded at 3-min intervals for 5,200 min in all sites apart from two (A and E). During the first spring 2024 burn period, sensors at A and E sites were removed after 3,100 min. Upon initial examination, this duration was inadequate; sensors were removed before soils returned to near-ambient temperatures. We modeled the missing portion of these time series using nonlinear regression fitted to the terminal 900 min of observed data, assuming exponential temperature decay consistent with the full 5,200-min records observed at other sites (Supplementary Methods).

To capture vertical heating at pile center, we inserted iButtons at 5, 10, 20, and 30 cm below the mineral soil surface (Brady et al., 2022). We created a pilot hole using a steel tool and manual T-post driver, then inserted the wooden stake assembly with embedded iButtons by hand (Supplementary Methods). Temperatures were logged at 3-min intervals for a minimum of 5,200 min, except at sites A and E as noted above.

Carbon and Nitrogen Accumulation and Loss Field Methods

We quantified C and N accumulation from pile derived materials and losses from the SOL by pairing measurements of pre-burn pools (pile biomass, SOL) with post-burn residual pools (pile remnants, charcoal, ash, SOL). Accumulation or loss for each component was computed as the difference between pre- and post-burn pools.

To estimate pile biomass and C, we first developed a mass–volume relationship from 11 piles not included in the main study which we randomly selected across the six sites to span the sampled volume range (1.00–11.85 m^3). For these 11 piles, we estimated volume (m^3) from linear dimensions, dismantled each pile piecewise, and measured total wet mass (kg) in the field (Supplementary Methods). Subsamples of fuel were taken from five within-pile locations, grouped by fuel size class (foliage/10-h, 100-h, large bole), and oven-dried the same day at 90°C until a constant mass was reached; gravimetric moisture content was used to convert field wet mass to dry biomass. We then fit a generalized linear mixed model (GLMM) with glmmTMB (Brooks et al., 2017) in R 4.5.0 (R Core Team, 2025), specifying pile volume and the fractions of fuels in the 1000-h and bole greater than 15 cm size classes as fixed effects. We applied a Gaussian error distribution with an identity link and conducted model reduction via Akaike's Information Criterion (AIC) comparing full versus reduced forms. Leave one out cross validation yielded RMSE = 32.30 kg, MAE = 26.13 kg, and $R^2 = 0.95$. Dry biomass was strongly predicted by pile volume (Supplementary Methods). We applied the derived relationship to all piles included in the study and assumed pile C mass to be 50% of oven-dry biomass, consistent with established woody fuel C fractions for boreal forests (Lamlom & Savidge, 2003).

To estimate pre-burn SOL C and N pools, we first measured pre-burn SOL depth as the mean of two depth measurements taken within 2 m of the pile edge at locations not affected by trampling during pile construction. To relate SOL depth to C and N pools, we collected five organic-soil monoliths per site in September 2024 at non-pile locations. Each monolith (10 cm ×

10 cm to full profile depth) was measured in the field, wrapped in aluminum foil, immediately frozen, and transported frozen to the laboratory. We halved monoliths longitudinally (archiving one half) and subdivided the other half into 5-cm increments. For each increment, we measured dimensions, weighed, homogenized by hand, removed coarse roots (> 2 mm), and oven-dried at 60°C to constant mass. No rocks were encountered. Dried increments were ground in a coffee mill (Krups, Solingen, Germany) and subsampled for elemental analysis to determine C and N concentrations. We converted these measurements into site-specific nutrient–depth models and then estimated organic-soil C and N pools per m² of burned area for each pile by combining those models with the measured pre-burn SOL depths. Model equations and parameter estimates are provided in Supplementary Table 1.

All post-burn measurements of C and N additions or losses were collected four days after ignition, prior to substantial dispersal or recovery processes. At each pile, post-burn SOL depth was measured at three points along a linear transect, one at the pile center and two at equidistant positions between the center and the pile edge to the north and south. The mean of these three measurements was taken as the residual SOL depth. Residual SOL C and N pools were estimated using the site-specific nutrient–depth relationships. Change in the SOL pools (kg element m^{-2}) were calculated as the pre-burn SOL pool minus the residual SOL pool.

To avoid the disturbed pile center (from prior thermocouple/iStake removal), we sampled ash and charcoal within a quadrat randomly offset 20 cm from the center in one of the four cardinal directions. Within each quadrat, we gently scraped all friable material with a trowel down to unburned substrate or mineral soil, then air-dried samples for three days, weighed them, and homogenized them through a 2-mm sieve. The coarse charcoal fraction was separated and weighed. Approximately 15 g subsamples of homogenized ash were oven-dried at 60°C until a constant mass was reached to determine moisture content and correct sample dry weight. For ash nutrient content, 20 ash subsamples were randomly selected for elemental analysis; mean contents were 10.34% C ± 1.29 and 0.349% N ± 0.087. Charcoal C content was not measured directly; instead, we used literature values, which were similar for conifers (78.41% ± 8.94) and hardwoods (78.57% ± 9.75). We adopted the mean across 35 reported values (78.50% ± 9.26) to estimate charcoal C content and compute charcoal C pools (Supplementary Table 2). Ash C and N and charcoal C contents were scaled to pools (kg element m^{-2}) by multiplying percent element by the quadrat sampling area (0.0484 m²).

We visually estimated the proportion of pile biomass not combusted (0–100) to assess completeness of combustion; uncertainty for this visual estimate was not quantified. For each pile and pool (pile C, SOL C and N, ash C and N, charcoal C), we paired pre-burn and post-burn estimates as described above and computed accumulation or loss as pre- minus post-burn values (with sign indicating direction), using the nutrient–depth models where applicable.

pH and Plant-available Nutrient Field Methods

At the end of the spring 2025 burn period, we deployed plant root simulator probes (PRS; Western Ag Innovations Inc., Saskatoon, SK) at four of six experimental sites (B, C, D, and F). We restricted deployments to these sites because each had both fall 2024 and spring 2025 pile burns, enabling measurement during the same first post-burn growing season for both treatments. Probes were installed vertically with the ion-exchange membranes centered 5cm below the soil surface. We placed three anion/cation probe pairs in each site type—fall pile burns, spring pile

burns, and adjacent unburned interspaces—for 62 days at all sites. At the end of the deployment, PRS probes were rinsed immediately with pressurized distilled water to remove residual soil, packaged, and sent to the Western Ag Innovations laboratory for analysis of 1 M KCl–extractable nutrients. Nutrient supply rates were calculated on the basis of ion-exchange membrane surface area and expressed as μg nutrient m^{-2} day^{-1}.

We also collected one surficial (0–5cm) soil grab sample at the time of PRS installation at each site. Samples were sealed in plastic bags and frozen until laboratory measurement of soil pH using a 2:1 deionized water:soil mixture.

Data Analysis

All data calculations and analyses were conducted in R version 4.5.0 (R Core Team). To visualize soil heating in space and time, we transformed temperature time-series from all vertical profile sensors into a depth-by-time matrix. At each three-minute recording interval we fit a natural cubic spline across depth in base R and predicted temperatures on a 0–30 cm grid at 0.1 cm increments; predictions at measured depths were replaced with the observed values.

We quantified soil heating with seven complementary metrics that capture intensity, exposure, and vertical penetration, rather than relying on a single biological threshold (following Pingree & Kobziar, 2019). Specifically, we computed maximum temperature (MaxT); exposure durations at three thresholds (Time25, Time300, Time500); cumulative heat load above two thresholds (CHL25, CHL50); and the maximum depth of mineral soil reaching 50°C (Depth50). Sensor level metrics (MaxT, Time25, Time300, Time500, CHL25, CHL50) were computed at each sensor depth (N = 285; Supplementary Figure 2), and the pile level metric (Depth50) was computed once per pile (N = 59). We defined baseline soil temperature as the mean of the first seven observations at the 10 cm sensor prior to ignition (Supplementary Figure 2).

We defined MaxT as the highest observed temperature at a sensor. We quantified thermal exposure as the total minutes with temperature ≥ 25, 300, or 500°C (Time25, Time300, Time500). To couple magnitude with duration, we calculated cumulative heat load above 25 and 50°C (CHL25, CHL50) by summing degrees above each threshold at every 3-minute step and converting degree-minutes to degree-hours (°C·h). These duration and heat load metrics distinguish brief, high-temperature pulses from longer, moderate exposures. We estimated vertical heat penetration with Depth50, defined as the deepest mineral soil depth to reach 50°C during the burn window. Using the spline based depth-time matrix at 0.1 cm resolution, we identified the deepest increment that exceeded 50°C at any time. Piles that never reached 50°C were excluded from this metric.

For C and N accumulation and loss, we evaluated charcoal C addition, ash C and N addition, SOL burn depth, SOL C and N losses, and change in belowground C and N. Net belowground C was defined as the pre-burn SOL C pool minus the sum of remaining SOL, ash, and charcoal C pools. We defined net belowground N as the pre-burn SOL N pool minus the sum of remaining SOL and ash N pools.

Using generalized linear mixed effects models (GLMMs; glmmTMB; Brooks et al., 2017) we modeled six sensor level soil heating metrics (MaxT, Time25, Time300, CHL25, CHL50) with fixed effects of burn season, pile volume, and pre-fire SOL depth and included sensor depth as a covariate. These models used random intercepts for pile nested within site to

capture within pile correlation and account for spatial dependency (Zuur et al., 2009). Time500 was not modeled due to the sparse number of exceedances. For the pile level penetration metric (Depth50), we fit the same fixed-effect structure but used a site-level random intercept only, reflecting a single estimate per pile. We restricted Time300 to surface sensors because subsurface sensors never reached 300 °C. Baseline soil temperature was analyzed with a GLMM including season as a fixed effect and a site random intercept.

For C and N responses, we modeled seven metrics (charcoal C, ash C and N, SOL burn depth, SOL C loss, and net changes in belowground C and N) using GLMMs with fixed effects of season, pile volume, and pre-fire SOL depth and their three-way interactions; all models included random intercept of site to account for spatial dependency (Zuur et al., 2009).

We screened all predictors for collinearity using variance inflation factors (VIF < 5; car; Fox et al., 2025) and confirmed non-collinearity. Model families and links were chosen to match response scales and distributional shapes, guided by residual plots and transformations when they improved fit and interpretability. Where diagnostics (*DHARMa*; Hartig et al., 2024) indicated improved fit of residuals, we included dispersion or zero inflation components. We compared the full model (with three-way interaction) to reduced models using AIC and favored the simpler model when $\Delta AIC > 2$, treating $\Delta AIC < 2$ as equivalent support; unsupported interactions were removed and models refit with main effects only (Zuur et al., 2009). After model reduction, we verified assumptions using simulated residuals via *DHARMa* and summarized fixed effects with estimates, standard errors, and Wald p-values; Supplementary Table 3 lists full specifications (family/link, random effects structure, and any dispersion or zero inflation terms). Post hoc comparisons used estimated marginal means (*emmeans*; Lenth et al., 2025) with a Tukey p-value adjustment. To visualize model results, we plotted conditional predictions from the final models holding covariates at their means. For sensor level soil heating metrics, we reported predictions at a reference depth of 15 cm, and for Depth50 and the C and C responses we held all covariates at their means.

To evaluate differences in plant-available soil nutrients and pH among control, fall, and spring burn conditions, we utilized a two step approach. We first evaluated nutrient specific responses by separately modeling each nutrient GLMM with fixed effects of treatment (control, fall burn, spring burn) and a random intercept of site. Post hoc analyses were conducted using estimated marginal means **(***emmeans*) with Tukey adjustment for multiple comparisons to test differences between treatments.

We then conducted a principal component analysis using base R *stats* to assess shifts in nutrient availability across treatments. Nutrient supply rates were transformed using a 1/log(p) transformation to reduce skewness and improve normality, then centered and scaled prior to analysis. To explicitly test for differences between fall and spring burns while accounting for site, we performed a distance based PERMANOVA on Bray–Curtis dissimilarities with permutations restricted within sites.

4. Results

Site Characteristics and Experimental Context

We examined 118 burn piles nested within six sites that captured a broad gradient in stand composition, SOL depth, and treatment and pile characteristics (Table 1). Overstory composition spanned mixed aspen–white spruce to white spruce dominated stands. Aspen was present at three sites (253–452 trees ha^{-1}), white spruce present at all sites (632–1,048 trees ha^{-1}), and black spruce was sparse or absent (0–234 trees ha^{-1}; Table 1). Soil organic layer depth ranged from 3.75 to 46 cm (Table 2). Relative to the 1,077 trees ha^{-1} prescription, residual densities varied by site (mean 1,093; range 645–1,424 trees ha^{-1}), with some sites thinned more heavily than prescribed and others left denser. Across all sites, pile density ranged from 41 to 62 piles ha^{-1} and mean pile volume from 3.57 (± 1 SE of the mean 0.24) to 5.66 (± 0.52) m^3 (Table 3).

Pile Combustion

Across the 59 piles instrumented for soil temperature, peak temperatures above baseline at the pile center mineral surface ranged from 1 to 817°C (Table 4). In every case, soil heating decreased rapidly with increasing soil depth, but this varied among sites and seasons (Supplementary Table 4, Supplementary Figure 4, 5, 6). We observed that the depth and duration of heating were greatest at sites A and B, minimal at sites E and F, and across all sites was greatest for fall compared to spring burns (Figure 1).

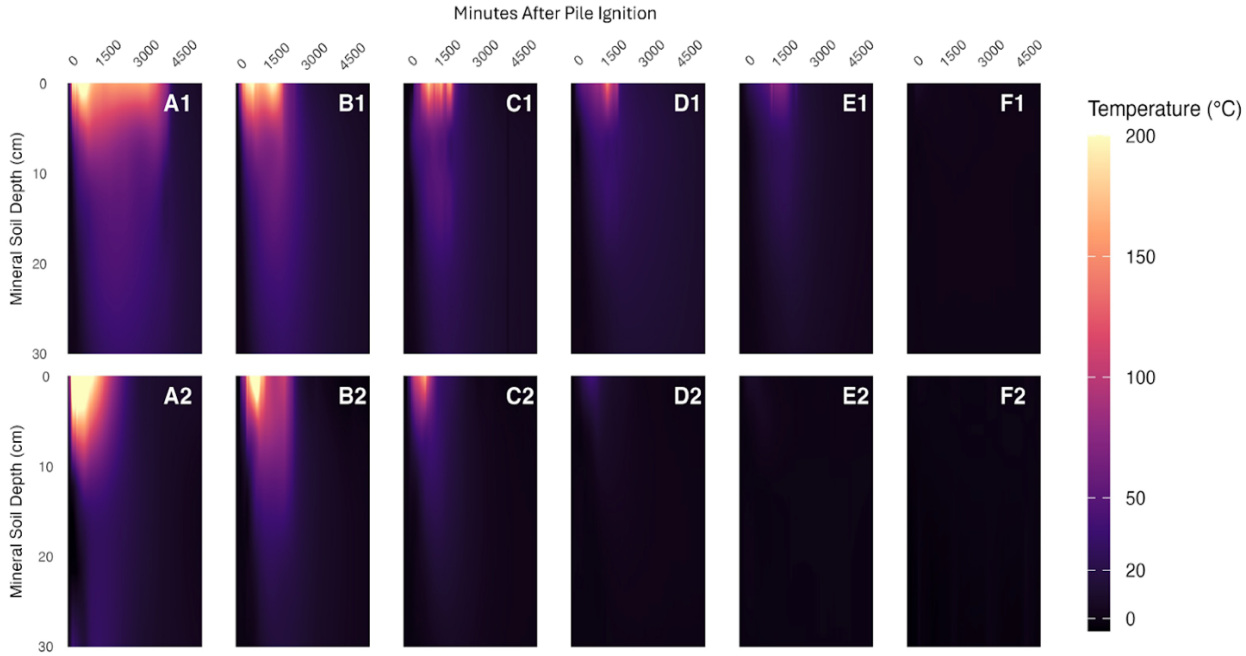

Figure 2. Heatmaps of soil heating beneath burn piles, averaged across five piles per site (four for panel D2). Each panel shows the duration and vertical extent of mineral soil heating at the pile center, with temperature indicated by color scale. Spring burns (panels labeled "2") generally exhibited shorter duration heating and shallower depth penetration than fall burns (panels labeled "1"). Panels represent average conditions.

Soil heating was concentrated at the pile center with little horizontal spread (Supplementary Figure 3). Across all piles, mean maximum temperature above baseline at the mineral soil surface was greatest at pile center (254 °C) compared to sensors located at the pile edge (48°C) and was lowest outside the pile perimeter (15 °C; Figure 2). No horizontal combustion spread ("creep") through roots or SOL was observed; the highest outside edge value was 37 °C, consistent with transient radiant heating during the flaming phase of pile combustion and well below temperatures required for combustion.

All piles completed flaming combustion within the first operational period, and no residual fire or heat was observed during post-burn surveys four days after ignition. Pile consumption was near complete across all sites and seasons (mean = 96.9%, median = 98%; N = 118).

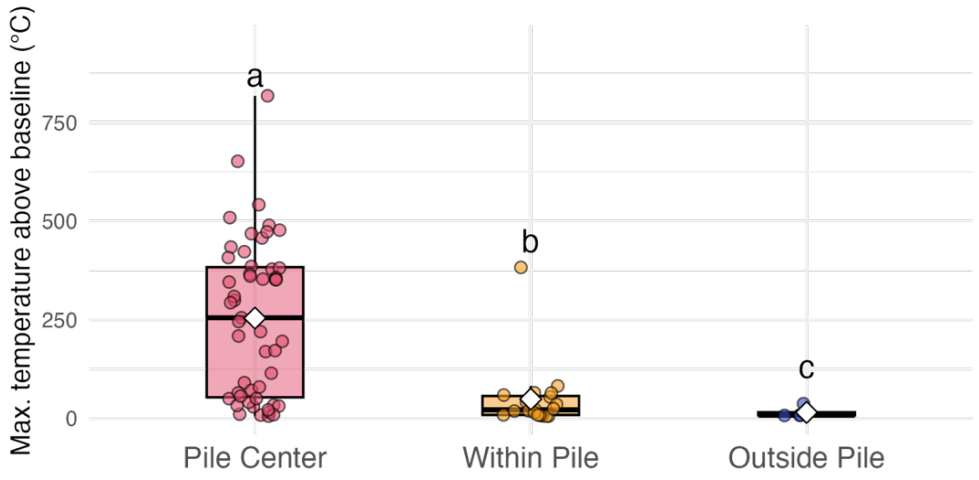

Figure 3. Maximum temperature above baseline at the mineral soil surface for sensors located at the pile center (N = 59), within the pile perimeter (N = 46), and outside the pile perimeter (N = 131; n = 59 piles). White diamonds indicate group mean and error bars show one standard deviation above the mean. Different letters indicate significant differences among groups ($F_{2, 71}$ = 19.005, $p<0.01$). The dashed vertical line represents the normalized pile edge.

Table 1. Mean (± SE) site and stand characteristics.

Site character	Units	Site					
		A	B	C	D	E	F
Mean elevation	m	498	535	10	656	634	646
Slope	deg	2	2	4	4	6	5
Aspect	deg	74	50	68	73	165	159
Aspen density	trees ha^{-2}	386 (±55)	452 (±104)	253 (±43)	0	0	0
Aspen basal area	m^2 ha^{-2}	4.47 (±0.62)	8.6 (±1.3)	4.27 (±0.83)	0	0	0
Mean aspen basal area	cm^{-2}	123 (±11)	255 (±30)	181 (±34)	0	0	0
White spruce density	trees ha^{-2}	1048 (±115)	703 (±64)	884 (±69)	729 (±81)	632 (±75)	928 (±92)
White spruce basal area	m^2 ha^{-2}	17.1 (±1.6)	9.37 (±0.85)	13.0 (±1.5)	10.6 (±1.0)	4.03 (±0.44)	3.57 (±0.35)
Mean white spruce basal area	cm^{-2}	173 (±11)	142 (±10)	163 (±23)	163 (±19)	72.5 (±9.0)	39.2 (±2.1)
Black spruce density	trees ha^{-2}	0	133 (±44)	0	0	133 (±44)	234 (±39)
Black spruce basal area	m^2 ha^{-2}	0	0.95 (±0.28)	0	0	1.22 (±0.04)	1.21 (±0.22)
Mean black spruce basal area	cm^{-2}	0	72.4 (±3.0)	0	0	105 (±38)	54.1 (±6.8)

Table 2. Mean (±SE) of soil organic layer, charcoal, and ash characteristics by site.

	Units	Site					
		A	B	C	D	E	F
Depth	cm	14.2 (±0.6)[a†]	14.6 (±1.2)[a]	15.2 (±0.7)[a]	18.8 (±1.0)[a]	28.8 (±1.4)[b]	33.3 (±1.8)[b]
Thaw depth	cm	na*	na	na	na	73.4 (±3.3)	57.5 (±2.59)
Bulk density	g cm^{-3}	0.07 (±0.01)	0.06 (±0.02)	0.06 (±0.01)	0.12 (±0.02)	0.09 (±0.02)	0.12 (±0.02)
Profile C	%	40.1 (±1.5)	40.5 (±1.2)	43.4 (±1.4)	39.9 (±1.4)	42.4 (±0.9)	42.2 (±1.5)
Profile N	%	1.22 (±0.04)	1.20 (±0.03)	1.15 (±0.06)	1.52 (±0.07)	1.30 (±0.06)	1.42 (±0.06)
Burn depth	cm	9.00 (±1.1)	14.07 (±1.1)	13.03 (±1.0)	12.72 (±1.0)	14.48 (±2.0)	9.22 (±1.7)
C pool pre-burn	kg C m^{-2}	2.54 (±0.17)	2.10 (±0.27)	2.36 (±0.18)	5.30 (±0.58)	8.43 (±1.61)	28.46 (±4.68)
N pool pre-burn	g N m^{-2}	42.7 (±3.5)	38.6 (±5.9)	36.3 (±3.4)	114.0 (±14.8)	213.9 (±57.9)	799.4 (±151.1)
C pool post-burn	kg C m^{-2}	0.94 (±0.23)	0.20 (±0.07)	0.41 (±0.08)	2.61 (±0.45)	5.62 (±1.23)	22.41 (±4.50)
N pool post-burn	g N m^{-2}	16.2 (±2.95)	4.9 (±0.2)	6.53 (±0.6)	20.5 (±1.9)	76.6 (±45.7)	273.3 (±85.2)
Ash C input	kg C m^{-2}	0.52 (±0.06)[a^]	0.50 (±0.05)[a]	0.36 (±0.04)[ab]	0.30 (±0.04)[bc]	0.27 (±0.04)[bc]	0.16 (±0.01)[c]
Ash N input	kg N m^{-2}	0.017 (±0.009)[a‡]	0.017 (±0.007)[ab]	0.012 (±0.006)[ab]	0.010 (±0.005)[bc]	0.009 (±0.005)[c]	0.005 (±0.002)[c]
Charcoal C input	kg C m^{-2}	0.27 (±0.10)[a+]	0.42 (±0.06)[ab]	0.64 (±0.09)[b]	0.35 (±0.04)[ab]	0.27 (±0.04)[a]	0.36 (±0.06)[ab]

† Different letters denote significant differences ($F_{5, 112} = 47.17$, $p<0.01$).

* Thaw depth is na when rocky soils prohibited manual probing.

^ Different letters denote significant differences ($F_{5, 107} = 10.45$, $p<0.01$).

‡ Different letters denote significant differences ($F_{5, 107} = 10.44$, $p<0.01$).

+ Different letters denote significant differences ($F_{5, 107} = 3.59$, $p<0.01$).

Table 3. Mean (±SE) pile characteristics by site.

	Units	Site					
		A	B	C	D	E	F
Density	piles ha^{-2}	40.75	59.4	49.5	53.6	61.88	57.43
Volume	m^3	4.33 (±0.25)^{ab*}	4.66 (±0.44)^{ab}	3.85 (±0.26)^{a}	5.66 (±0.52)^{b}	3.66 (±0.37)^{a}	3.57 (±0.24)^{a}
Large wood fraction	%	48 (±3)	57 (±5)	44 (±3)	47 (±6)	42 (±5)	39 (±3)
CWD fraction^{+}	%	0.25 (±1)	1.5 (±1)	0.4 (±2)	0	0	0
Fuel moisture fall^{+}	%	25.9 (±1.4)	40.9 (±3.1)	45.3 (±3.2)	45.4 (±3.4)	24.0 (±0.7)	40.4 (±2.8)
Fuel moisture spring^{+}	%	28.1 (±2.4)	36.4 (±4.0)	36.0 (±1.6)	31.2 (±1.9)	25.2 (±1.4)	27.3 (±0.4)

* Different letters denote significant differences ($F_{5, 112} = 4.57$, $p<0.01$).

$^{+}$ Coarse woody debris (CWD) is dead wood that was not standing at the time of pile construction.

$^{+}$ Fuel moisture measured at five piles per site per season.

Table 4. Mean (±SE) soil heating values by site.

Soil heating metric	Units	Site					
		A	B	C	D	E	F
MaxT†	°C	412.5 (±57.2)	399.1 (±37.6)	292.7 (±51.0)	134.7 (±46.7)	53.7 (±21.2)	6.9 (±3.2)
Time25†	min	2705.7 (±429.7)	1878.3 (±268.2)	1554.9 (±185.2)	1202.3 (±291.3)	672.6 (±289.1)	18.0 (±18.0)
Time300†	min	756.6 (±200.1)	351.0 (±111.9)	72.9 (±30.3)	25.7 (±17.1)	0	0
Time500†	min	35.7 (±35.7)	6.3 (±5.1)	0	0	0	0
CHL25†	°C·hr	7321.5 (±1578.9)	4488.1 (±822.1)	2302.9 (±348.1)	1014.8 (±436.2)	491.3 (±260.5)	1.4 (±1.4)
CHL50†	°C·hr	6381.3 (±1445.3)	3786.2 (±739.4)	1737.2 (±310.4)	675.7 (±336.0)	274.6 (±161.7)	0
Depth50+	Pr(soil ≥ 50°C)	1.0 (±0.0)	1.0 (±0.0)	1.0 (±0.0)	0.6 (±0.2)	0.3 (±0.2)	0
Depth50*	cm	20.9 (±2.1)	14.6 (±1.9)	10.2 (±2.1)	6.2 (±2.6)	6.3 (±2.3)	na

† Values from sensors located at the pile center at the mineral soil surface (0 cm mineral soil depth; N = 59).

+ Probability of soil heating reaching at least 50°C at any measured depth (N = 59).

* Mean mineral soil depth to reach the 50°C threshold given that soil heating did reach or exceed 50°C at any measured depth (N = 37). When soil heating did not reach or exceed 50°C in any piles, Depth50 occurrence is 0 and Depth50 is shown as na.

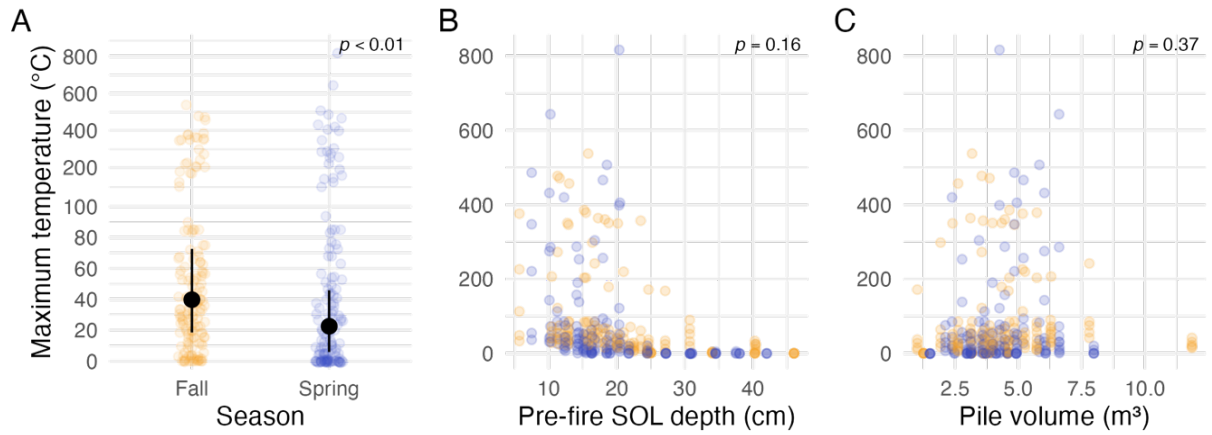

Figure 4. Maximum soil temperature (°C) during pile burns. Panels summarize a generalized linear mixed model (GLMM) fit to sensor level data (N = 285). Y-axis limits and breaks in panel A are tuned for readability of predictions and raw data. Panels show model predicted effects for predictors that were significant in the GLMM; non-significant predictions are omitted. Black dots (with 95% CI whiskers) are predictions with other covariates held at their sample means and sensor depth fixed at 15 cm; p-values are printed.

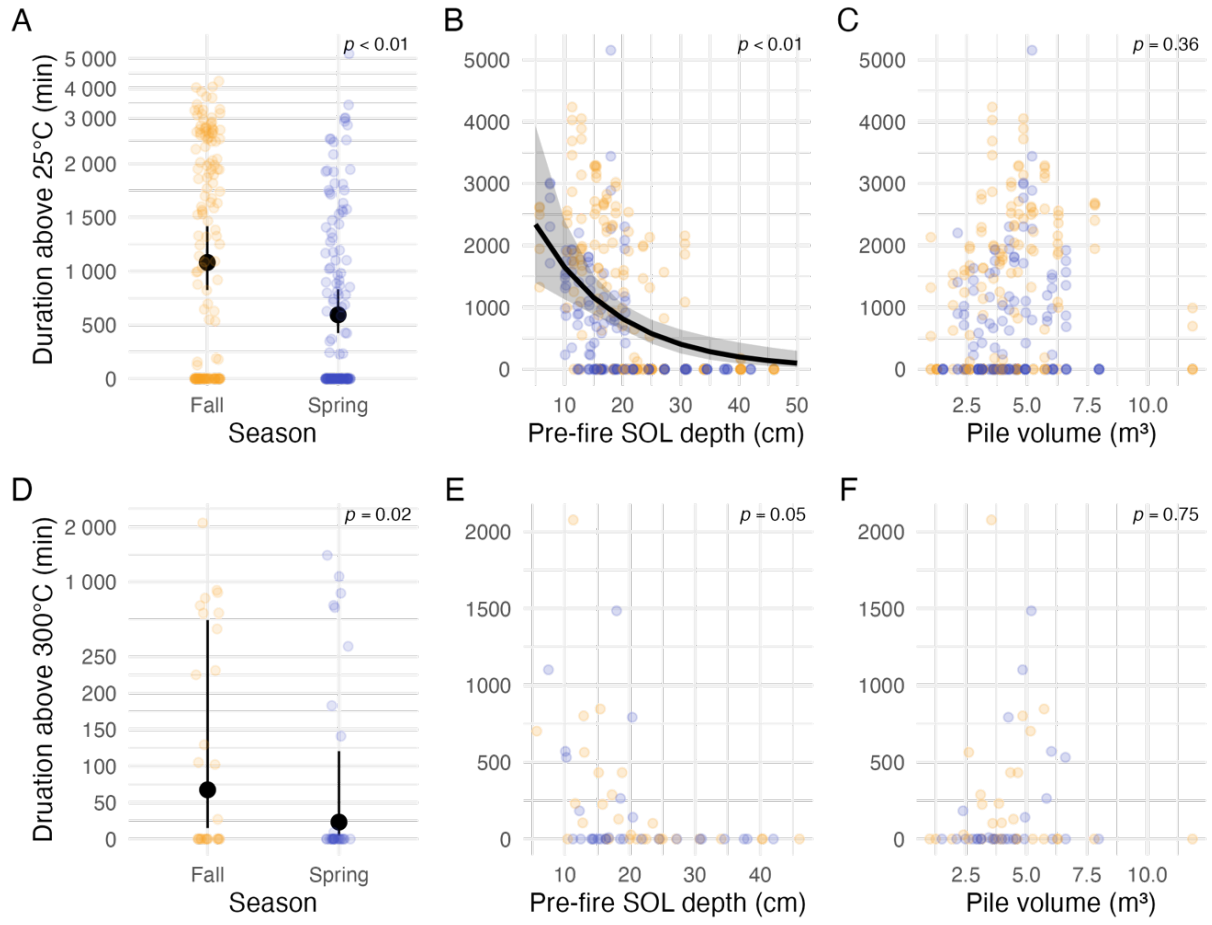

Figure 5. Duration above 25 and 300°C (minutes) during pile burns. Panels summarize a generalized linear mixed model (GLMM) fit to sensor level data (N = 285). Y-axis limits and breaks in panels A and D are tuned for readability of predictions and raw data. Panels show model predicted effects for predictors that were significant in the GLMM; non-significant predictions are omitted. Black dots (with 95% CI whiskers) are predictions with other covariates held at their sample means and sensor depth fixed at 15 cm; p-values are printed.

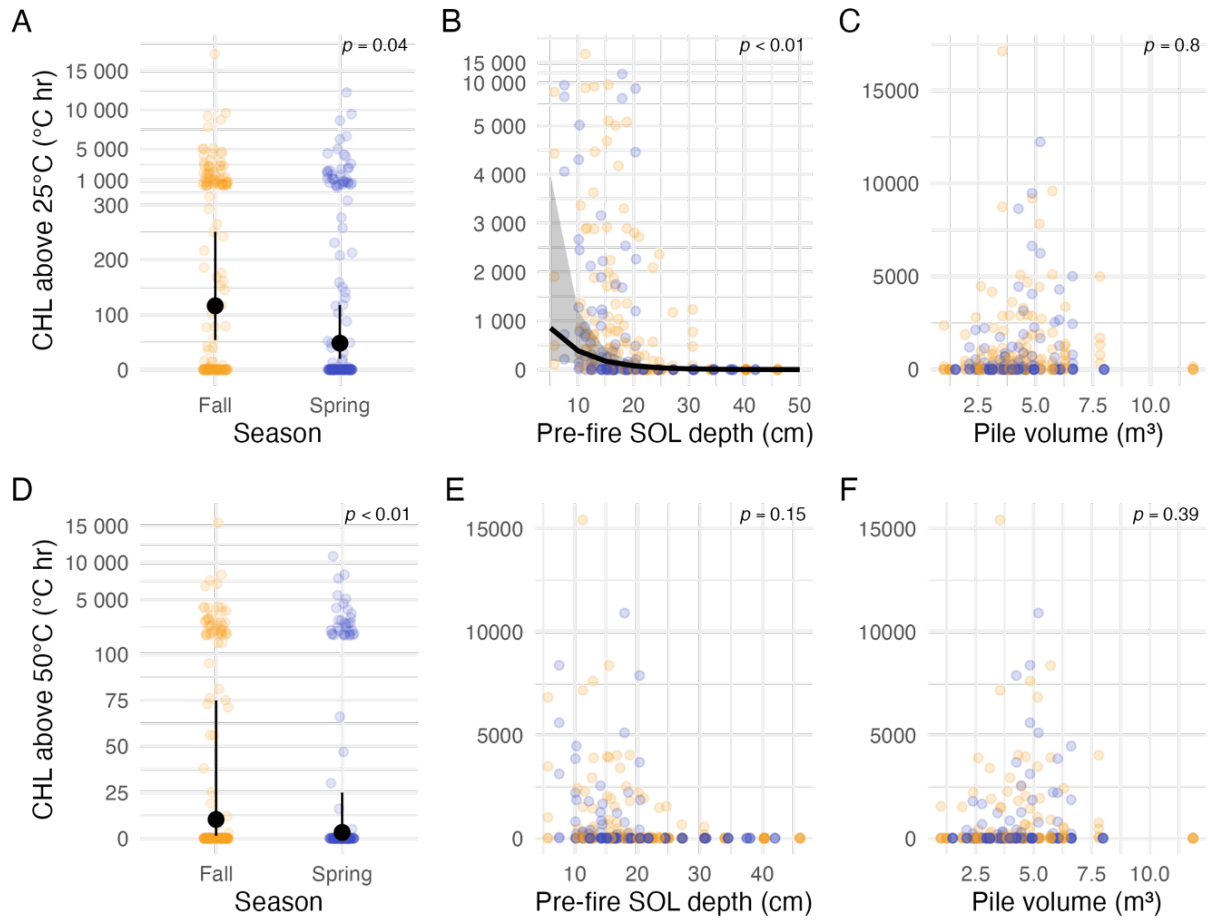

Figure 6. Cumulative heat load above 25 and 50°C (°C·hrs) during pile burns (n = 59). Panels summarize a generalized linear mixed model (GLMM) fit to sensor level data (N = 285). Y-axis limits and breaks in panels A, B, and D are tuned for readability of predictions and raw data. Panels show model predicted effects for predictors that were significant in the GLMM; non-significant predictions are omitted. Black dots and lines (with 95% CI whiskers and ribbon) are predictions with other covariates held at their sample means and sensor depth fixed at 15 cm; p-values are printed.

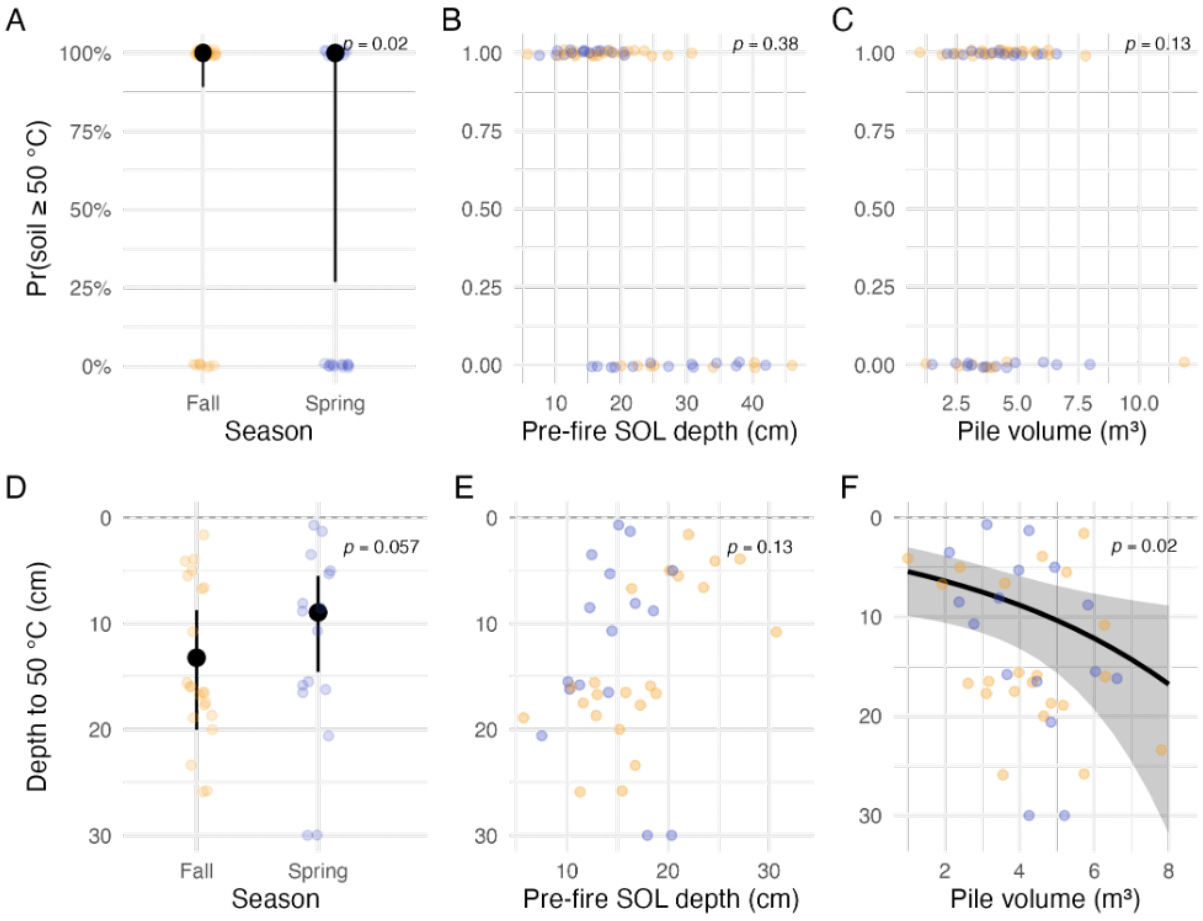

Figure 7. Depth to reach 50°C (N = 59 piles) analyzed with a two part generalized linear mixed model hurdle framework. Panels A–C present the occurrence component: estimation of the probability that soil temperatures reached ≥ 50°C. Panels D–F represent the conditional component: a mixed model fit only to piles where ≥ 50°C occurred, estimating the deepest soil depth that reached 50°C. Black points and lines with 95% confidence ribbons are model predictions; raw observations are shown as colored points. For all predictions, other covariates are held at their sample means. Predictions are displayed only for predictors significant in the corresponding model; p-values are printed.

Soil Heating Metrics

The six metrics of SOL heating we examined showed similar responses to our hypothesized driver of season, but less consistently responded to SOL depth and pile volume. For all metrics apart from Depth to reach 50 °C, soil heating was higher in the fall than spring: at 15 cm mineral soil depth, maximum temperature averaged 39.7°C in fall vs. 22.6°C in spring, and time > 25°C was 82% greater in fall (Figure 3A, 4A, 5A; Supplementary Table 4). The Depth to 50°C estimate, while not statistically significant, was directionally consistent with this pattern (Figure 6A & 6D; Supplementary Table 4).

Greater pre-fire SOL depth reduced soil heating for the lower temperature thresholds of CHL 25 and Time25. Increasing pre-fire SOL depth from 0 to 50 cm reduced cumulative heat load above 25°C by 99% and time above 25°C by 70% (Figure 4B, 5B). Pre-fire SOL depth did not significantly impact the remaining metrics (MaxT, Time300, CHL50, and Depth50; Supplementary Table 4). Most heating metrics were not impacted by pile volume. The only exception was depth to 50 °C, where every additional m^3 of pile volume increased the depth to 50°C by 17.5% (Figure 6F). We recorded a duration above 500°C at only three of 285 sensors, where the maximum duration above threshold was 357 minutes at a pile in site A.

We found baseline soil temperature differed by season: mean fall soil temperature was above 0°C (0.35 ± 0.16°C) and mean spring soil temperature was below well 0°C (−1.89 ± 0.16°C; Supplementary Table 4)

Carbon and Nitrogen Accumulation and Loss

Contrary to our expectations, fall burns caused nearly threefold larger reductions in belowground C than spring burns (0.99 ± 0.36 vs 0.39 ± 0.36 kg C m^{-2}; Figure 7A; Supplementary Table 5). We also observed deeper SOL burn depths in Fall compared to spring (Figure 7F) and larger SOL C losses as burn depth increased (Figure 7H). Charcoal additions did not differ by season (Figure 7C).

We next examined how pre-fire SOL depth and pile volume shaped these outcomes. Change in belowground C varied with both factors, with volume modifying the SOL-depth effect (Figure 7B). As SOL depth increased, change in belowground C became more negative, and the decline was steeper when piles were larger. Averaged over season, each 10 cm increase in SOL depth was associated with an additional 0.98 ± 0.42 kg C m^{-2} loss in the upper-quartile pile volume compared with the lower-quartile volume (Figure 7B). Model predictions also indicate a shift at 15 cm pre-fire SOL depth: shallow SOL depths tended to show net C gains, while deeper SOL depths showed net C losses (Figure 7B).

Supporting patterns aligned with these trends. Soil organic layer burn depth increased with pre-fire SOL depth and was greater for larger piles; at 40 cm pre-fire SOL depth, upper-quartile volumes burned 7.9 ± 2.8 cm deeper than lower-quartile volumes (Figure 7G). Averaged over season and at mean pile volume, SOL C losses increased by 33.5% for each 10 cm increase in pre-fire SOL depth (Figure 7I), indicating that as piles burn deeper and resulting SOL C losses becomes larger, belowground losses overtake aboveground inputs from ash and charcoal.

Inputs from pile combustion were limited, charcoal addition did not differ by season (Figure 7C), showed no clear relationship with SOL depth (Figure 7D), and declined with

increasing pile volume by 0.059 ± 0.022 kg C m^{-2} per every cubic meter (Figure 7E). Ash C inputs were unrelated to season, pre-fire SOL depth, or pile volume (Supplementary Table 5).

Change in belowground N was nearly twice as large in fall than spring (-37.6 ± 12.7 vs -21.6 ± 9.3 g N m^{-2}; Figure 8A; Supplementary Table 5). Belowground N losses increased in magnitude with pre-fire SOL depth: at 10 cm our model predicted -6.7 ± 8.9 g N m^{-2}, whereas at 40 cm it predicted -253.4 ± 105.1 g N m^{-2} (Figure 8B). Contrary to our expectation, pile volume was not a significant predictor of net belowground N (Figure 8B; Supplementary Table 5). Ash N inputs were unrelated to season, pre-fire SOL depth, or pile volume (Supplementary Table 5).

pH and Plant-available Nutrients

Consistent with our expectation, we found higher soil pH after fall burns than spring burns (7.40 ±0.31 vs. 6.25 ±0.31; $p<0.01$; Figure 9; Supplementary Table 6). Pile burning produced soils with large, consistent increases in individual nutrients relative to unburned control soils and these increases did not differ by season (Figure 9; Supplementary Table 6). Ammonium and nitrate were several-fold higher (+274% and +554%), phosphorus increased the most (+810%), and potassium and calcium also rose sharply (+277% and +354%; Table 5). Multivariate patterns echoed and refined this result. Our principal component analysis showed burned soils clustering apart from controls along the primary nutrient-availability axis (PC1). Burned soils scored higher on PC1, consistent with increases in sulfur, magnesium, and calcium (Figure 10; Supplementary Table 7). While individual nutrients did not show season effects (Figure 9), when all nutrients were included, a small seasonal difference was detected (Figure 10; post hoc PERMANOVA; $R^2 = 0.025$, $F = 1.91$, $p = 0.03$). Increases in ammonium and potassium were more associated with the spring season and increases of calcium and aluminum aligned more with the fall season (Figure 10).

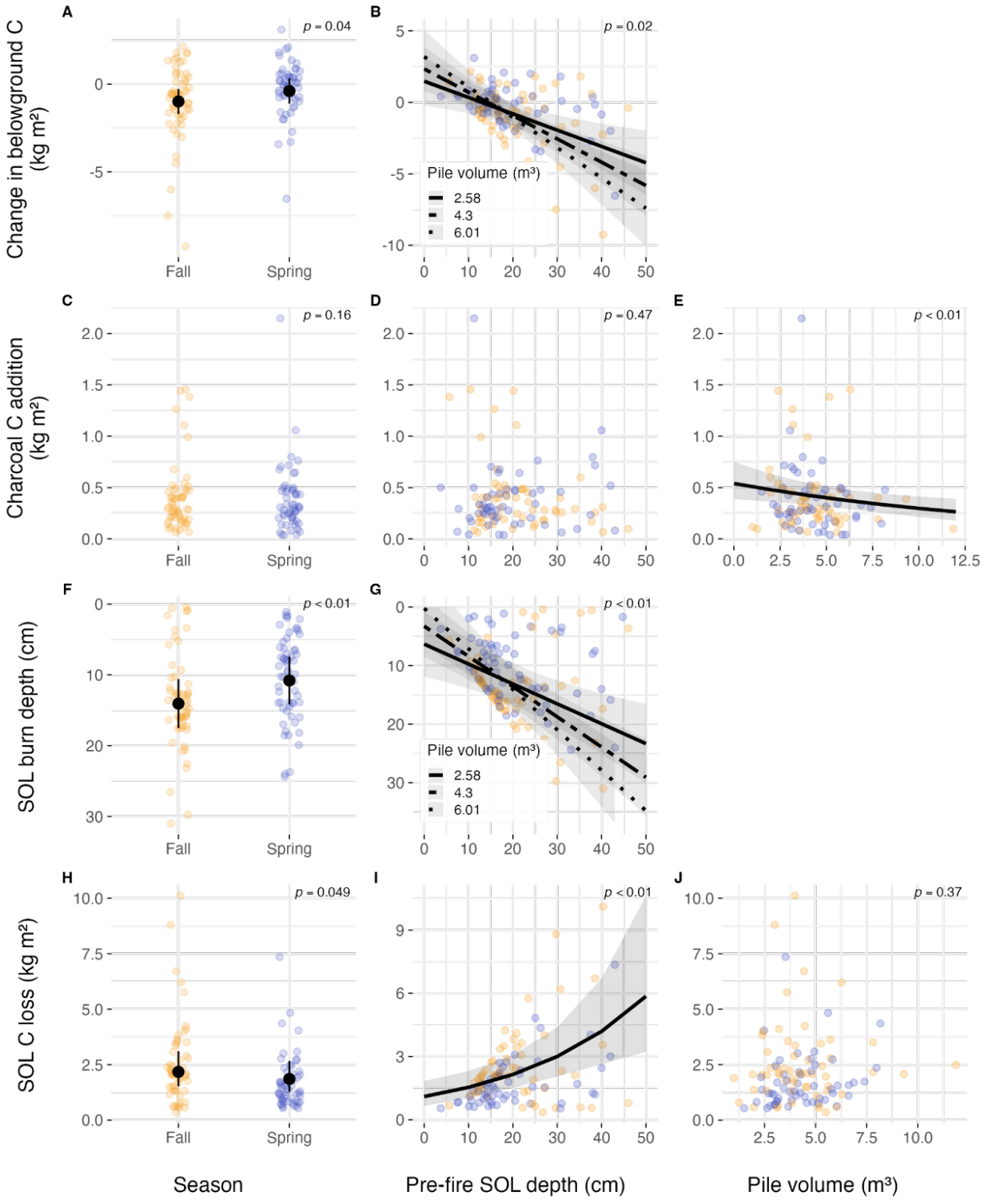

Figure 8. Change in belowground C balance and components within pile footprint (N = 118 piles). Points are pile level observations (colored by season); black symbols/lines with shaded ribbons are model are printed on panels. For partial effects, other covariates are held at their sample means. Where interactions with pile volume are shown, pile volumes are plotted at lower quartile, mean and upper quartile.

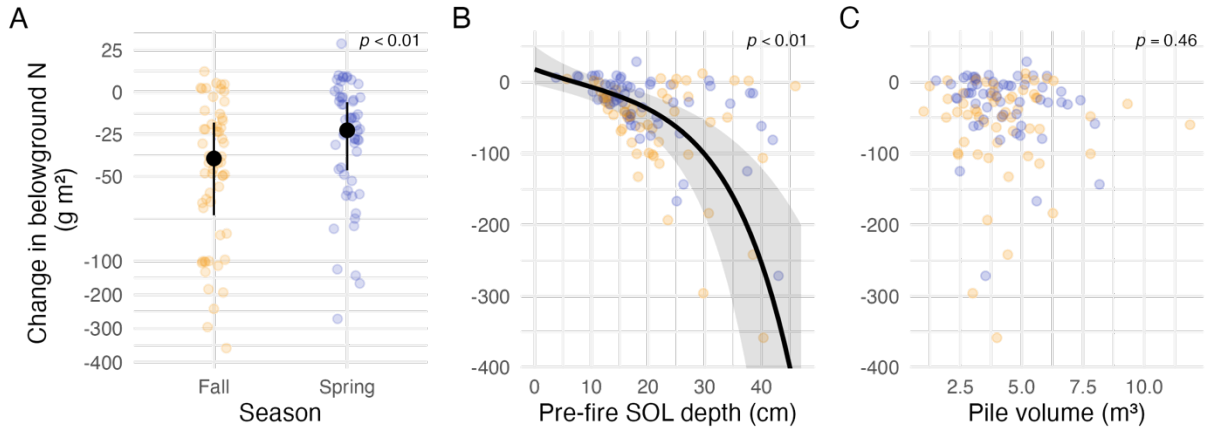

Figure 9. Change in belowground N balance within pile footprint. Points are pile level (N =118) observations colored by season; lines with shaded ribbons are model predictions with 95% confidence intervals from generalized linear mixed models. For partial effects, other covariates are held at their sample means. P-values are printed on panels.

Table 5. Mean (±SE) nutrient supply rate (µg nutrient 10cm^{-2} day^{-1}) by site.

Nutrient	**Site**							
	B		**C**		**D**		**F**	
	Burned	*Control*	*Burned*	*Control*	*Burned*	*Control*	*Burned*	*Control*
Nitrate	8.2 (±4.1)	0.63 (±0.3)	20.0 (±5.7)	2.54 (±0.8)	22.0 (±4.2)	3.4 (±1.1)	9.1 (±1.9)	2.69 (±0.8)
Ammonium	29.5 (±4.2)	2.4 (±1.0)	37.5 (±6.8)	6.7 (±1.8)	42 (±11)	14.3 (±3.8)	6.1 (±1.6)	4.6 (±1.8)
Phosphorus	68.7 (±8.7)	7.7 (±1.5)	57.8 (±6.2)	4.76 (±0.64)	44.0 (±5.8)	5.1 (±1.6)	49.7 (±5.6)	7.0 (±2.1)
Potassium	1694 (±156)	331 (±77)	1945 (±198)	303 (±42)	465 (±141)	367 (±62)	997 (±228)	315 (±72)
Calcium	782 (±74)	213 (±68)	608 (±67)	116 (±11)	1706 (±146)	408 (±115)	1896 (±166)	353 (±107)
pH	6.89 (±0.33)	5.82 (±0.19)	6.04 (±0.35)	5.52 (±0.11)	6.41 (±0.31)	5.67 (±0.19)	7.88 (±0.27)	5.46 (±0.18)

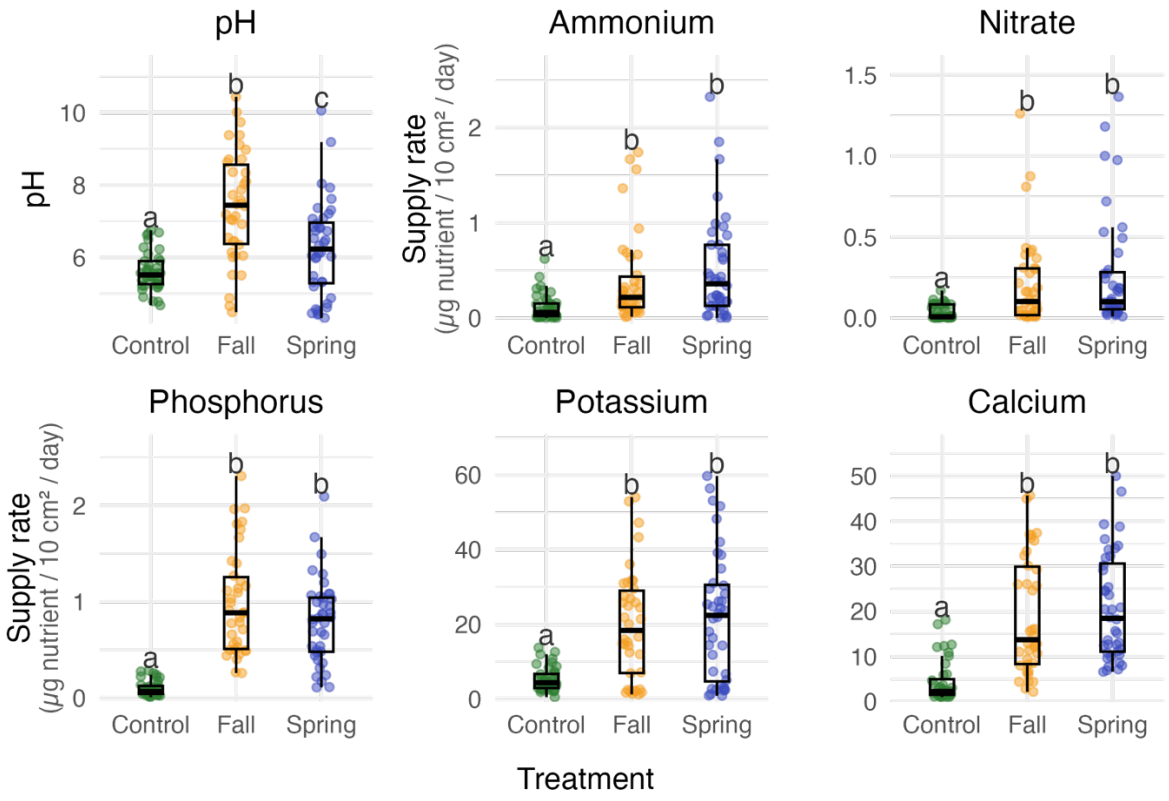

Figure 10. Plant-available nutrient supply rates by treatment. Each panel displays PRS probe–derived nutrient supply rates across Control, Fall burn, and Spring burn treatments. Points are individual samples pooled across sites and jitter added to show within group dispersion. Letters above boxes come from post hoc comparisons of treatment means and denote groups that differ at adjusted $p < 0.05$; letters are derived from generalized linear mixed effects models fit separately for each nutrient and pH.

5. Discussion

Hand thinning followed by pile burning is a key management strategy for fuel reduction and wildfire risk reduction in boreal forests. In this study, we examined 59 burn piles across six sites in Interior Alaska to assess how season (frozen versus thawed), pre-fire SOL depth, and pile volume impact the magnitude, duration, and penetration of soil heating and an additional 59 piles for soil C and N pools, plant nutrient availability, and soil pH. We found that heating remained shallow and confined to the pile footprint and that season had the strongest influence on soil responses, with spring burns limiting heating and belowground C loss compared to fall burns. Pile burns showed a clear early nutrient pulse and higher pH, with pH tending to be highest after fall burns. Together, these findings provide a clear evidence base to guide near term planning to reduce wildfire risk while anticipating soil impacts, and, over time, support regeneration, strengthen landscape stewardship, and help communities live well with fire.

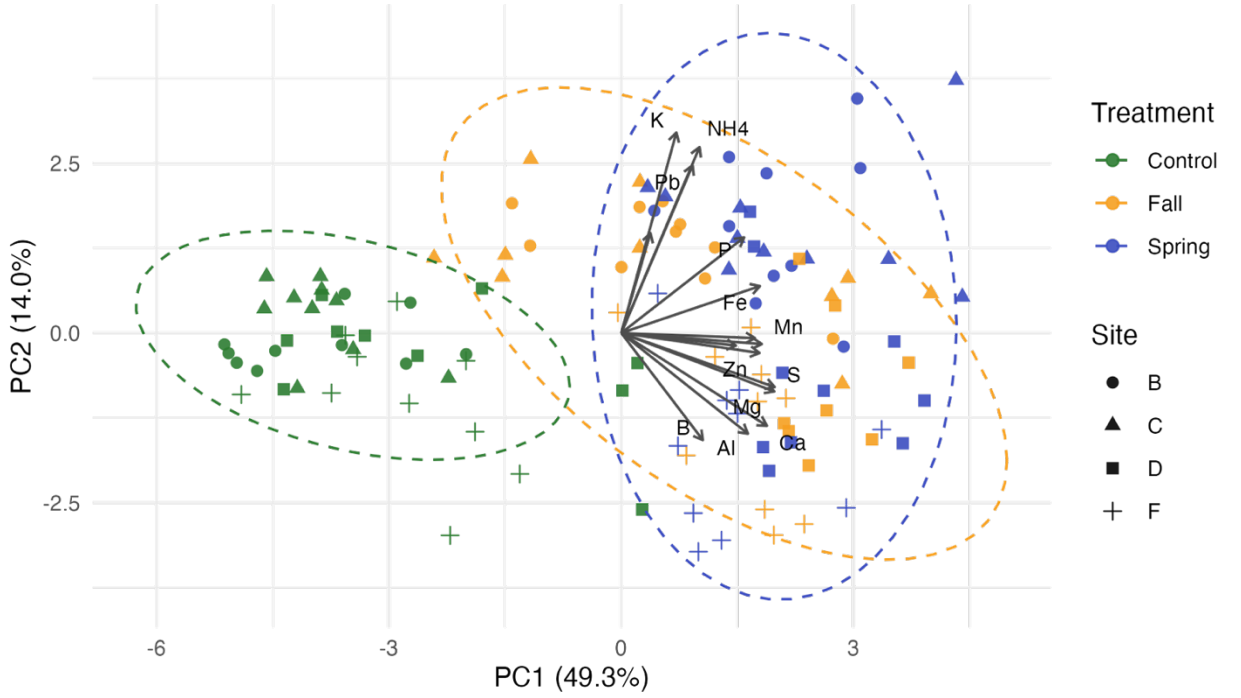

Figure 11. Principal components analysis of plant-available nutrient supply rates (µg nutrient $10cm^{-2}$ day^{-1}) measured with PRS probes. At each of four sites (B, C, D, F), we collected 30 samples (10 Control, 10 Fall, and 10 Spring) yielding 120 samples in total; a sample is the mean of three PRS probe pairs from the same treatment at a site. Each point is one sample, colored by treatment and shaped by site; dashed outlines are 95% data ellipses for each treatment. The ordination shows the first two principal components, explaining 63.3% of variance. Black arrows are variable loading vectors projected onto the PC1–PC2 plane; arrow direction indicates increasing nutrient values and arrow length reflects association strength with the axes. Labels mark the highest loading nutrients.

Magnitude and Duration of Heating

Heating beneath piles was characterized by high near surface temperatures and exposures lasting from hours to days that were shaped primarily by season and pre-fire SOL depth. Maximum temperatures between 700 and 800°C were comparable to values reported for pile burns and "mega-logs" in the Western US (Busse et al., 2013; Smith et al., 2016). Maximum temperatures declined as pre-fire SOL depth increased, indicating that thick organic horizons acted as strong thermal buffers. Maximum temperature alone, however, is not sufficient to evaluate biological effects on plant roots and microbial communities (Pingree & Kobziar, 2019). Soil organisms respond to both intensity and exposure time. To capture these rate-dependent processes, we analyzed metrics that integrate temperature and time.

For biologically relevant lower temperature thresholds, we evaluated duration and cumulative heat load above 25°C as conservative indicators that bracket the extreme range of mineral soil temperatures expected in Interior Alaska outside of fire (Bonanza Creek Long-Term Ecological Research Program Climate Database, 2025). We also examined cumulative heat load

above 50°C as a more liberal threshold near the naturally occurring upper range of soil temperatures. Interpreting these thresholds for soil biota, exposures above 25°C likely represent novel thermal conditions for boreal soils that rarely, if ever, occur outside of summer wildfires. As time or cumulative heat load above these thresholds increases, impacts to fine roots and microbial communities are expected to increase through thermal stress, membrane and enzyme disruption, and moisture loss that can accompany heating (Pingree & Kobziar, 2019). Longer or larger cumulative exposures at 25 or 50°C therefore indicate greater potential for reductions in microbial activity, root function, and mycorrhizal integrity at the depths where they occur, whereas shorter, more buffered exposures suggest more limited biological impacts, especially where deeper SOL depths or frozen soil constrain heat penetration.

To connect heating to nutrient change mechanisms, we assessed durations above 300°C and 500°C, which correspond to temperatures where ammonium volatilization and phosphorus mineralization become likely. Durations exceeding 300°C and especially 500°C were uncommon and generally brief. This pattern suggests that our observations of elevated nutrient supply rates are better explained by ash deposition and associated base cation inputs than by sustained in situ thermal transformations of N or P within the soil. As ash inputs to burned soils diffuse and diminish in concentration with time, this may result in substantial net N losses within pile burns.

Spatial Extent of Heating

Pile burning produced shallow heating confined to the pile footprint, with no lateral combustion creep. This pattern aligns with theory and observation that soils conduct heat poorly, so detrimental impacts, when they occur, are typically restricted to surface layers (Busse et al., 2010, 2013; Massman & Frank, 2004). Because these horizons contain most fine roots and microbial biomass, intense but localized heating under piles likely causes high mortality, yet the small footprint and sharp thermal gradients should allow recolonization from unburned soil and vegetation at the pile edge. Energy partitioning during combustion reinforces this interpretation, with most heat lost upward and only a small fraction penetrating downward to the soil profile (Hungerford et al., 1991), which explains the rapid vertical attenuation with depth.

Heating was generally greatest near pile centers and declined toward edges, consistent with prior research in pile burns (Busse et al., 2013). We observed no horizontal spread through litter, roots, or organic soils. The few outside edge signals were low temperature (< 37°C) and brief, consistent with short lived radiant heating during the flaming phase of pile combustion rather than conductive or smoldering spread. These instances occurred where a very shallow snowpack (less than 3 cm) quickly melted and exposed the soil surface (personal observation). Our findings may not extend to snow free ignitions or to periods with sustained wind that could alter convective and radiant heating. Lateral effects under those conditions remain an uncertainty. Taken together, limited vertical penetration and minimal horizontal spread indicate low risk to soil biota beyond the immediate pile area. Risk is lowest when burns occur in spring over frozen soils, when SOL depth is greater 25cm, and with a snowpack greater than 3cm, which collectively restrict vertical heating and curtails brief outside edge warming.

Carbon and Nitrogen Addition and Loss

The primary driver of in belowground C and N pools was SOL burn depth, which was strongly influenced by season for both C and N and additionally by pile volume for C. Soil organic layer burn depths were comparable to the 13 to 15cm values reported for Alaskan

wildfires across forest types (Mack et al., 2021), indicating that the concentrated fuels in piles do not necessarily produce unusually deep combustion. Full consumption of the SOL was rare once pre-fire thickness exceeded 25cm. If burn depth were controlled primarily by fuel loading and heat release from the pile, we would expect thick organic layers to be fully consumed; instead, combustion consistently self-limited in deeper organic soils. This pattern points to organic soil moisture as a key constraint on organic layer burn depth and smoldering (Miyanishi & Johnson, 2002), since organic soils in fall and spring are typically wetter than during summer wildfire conditions. A primary limitation of this research is that we did not directly measure soil moisture beneath piles prior to ignition, though moisture strongly influences heating dynamics and burn depth (Massman et al., 2010). Future work that incorporates pre-burn soil moisture, or that couples continuous moisture sensing with temperature profiles, will help separate these effects.

Carbon balance shifted with organic layer thickness; when SOL depth was less than 15cm, ash and charcoal inputs from piles outweighed SOL C losses, producing positive net belowground C. When SOL depth exceeded 15cm, deeper burn depths drove net C to become negative. Larger piles intensified these negative balances by burning farther into the SOL, particularly where pre-fire SOL depth exceeded 20cm. Seasonal contrasts in net belowground C were best explained by differences in SOL burn depth rather than differences in ash or charcoal production, with fall burns creating larger net C losses. Although absolute changes to belowground C were small, their direction with respect to SOL depth is operationally important. Practitioners aiming for stand conversion from conifer to aspen dominance may accept deeper organic layer consumption and larger net C losses to create conditions which promote aspen and birch germination. Practitioners seeking to minimize disturbance to C pools at the site level should favor smaller piles and spring burning when placing piles where SOL depth is greater than 15cm.

Changes to belowground N mirrored the seasonal and pre-fire SOL depth patterns observed for C, however, nearly all piles produced N losses. The magnitude of these losses is comparable to post-wildfire patterns in Alaska (Alexander & Mack, 2016), which again indicates that operational pile burning does not exceed typical wildfire effects. Nitrogen is readily volatilized at temperatures near 300 °C, which are commonly reached as fuels combust. As a result, the concentration of N in ash is very low, and charcoal contains very little (<0.1%) N (Antal & Grønli, 2003). Without meaningful soil N inputs from pile combustion, practitioners should avoid placing them where the SOL is deep or on hummocks. When retaining organic layer N is a priority, select spring windows with frozen soils, site piles on thinner or moist organic layers or small mineral patches, and prepare footprints to limit smoldering into the organic horizon so that more N is retained at the site.

Two uncertainties apply to the addition and loss estimates we presented here. First, because we did not quantify pre-burn SOL moisture, we could not directly test how moisture modulated SOL burn depth. Second, although we interpreted net belowground balances using ash and charcoal inputs versus SOL C losses, our study did not track post-burn redistribution of ash beyond the footprint (e.g. during combustion via wind transport). Future work incorporating these mechanistic processes may be better able to identify the environmental drivers of the changes to these nutrient pools.

Practically, decisions about season and pile construction should be coupled to SOL depth at individual piles. Schedule burns under colder soil temperatures and moderate pile volume in

thick organic settings to limit belowground losses. Where organic layers are shallow, there is an opportunity to capture ash and charcoal inputs with fewer net losses of C and N, regardless of season.

pH and Plant-available Nutrients

Plant-available nutrients and soil pH shifted rapidly after pile burning, creating near term conditions likely to influence early recovery through fertilization and alkalization. These effects are consistent with an ash-bed effect (Knoepp et al., 2005): ash deposition to the soil increases the concentration of base cations and carbonates, elevating pH and increasing the availability of ammonium, nitrate, phosphorus which is consistent with findings of others (Creech et al., 2012).

Relative to unburned soils, prior work on pile burns documented higher soil pH and ammonium but did not report consistent increases in other nutrients (Johnson et al., 2011). In contrast, our measurements showed consistent post-burn increases not only in pH and ammonium but also in nitrate, phosphorus, potassium, and calcium. We attribute this difference to sampling timelines and ash immobilization. For spring burns, resin probes were deployed within six days of ignition, capturing the initial nutrient pulse. For fall burns, sampling occurred four months after ignition under winter snowpack and with frozen soils that likely inhibited leaching and lateral transport. We suggest this preserved an early pulse signal in the plant-available nutrient pool until snowmelt when soils begin to thaw. While this design helped preserve early signals, it also limits inference about the full temporal trajectory of the pulse. Repeated resin deployments through the first two years of soil and vegetation recovery would clarify pulse duration.

Multivariate analyses clearly separated burned from unburned soils, and seasonality was detectable at the multivariate level. Univariate tests, however, showed large increases in nutrient supply rates for both burn seasons relative to controls with no difference between fall and spring. Taken together, these results point to the primary ecological signal being the contrast between burned and unburned soils, with increases in burned soil nutrient supply rate ranging from one to nine times greater than control soils. Soil pH exhibited a large treatment effect, with fall greater than spring and spring greater than control. Because charcoal and ash inputs did not differ by season, the higher pH following fall burns most likely reflects greater post-burn dispersal and incorporation of base cations into the soil matrix.

These findings identify an initial operational window in which nutrient-rich conditions in pile burns can be used to guide regeneration toward desired community composition or structure. Practical applications include timing seeding or planting to coincide with the nutrient pulse (Thorpe & Timmer, 2005), prioritizing early surveillance and control of invasive plants that may capitalize on elevated fertility, and, where the risk of nutrient export is high, mechanically incorporating ash and charcoal into the soil to slow runoff and reduce losses. Accordingly, treatment planning should emphasize the strong burned versus unburned contrast and the increased pH observed after fall burning when setting regeneration objectives for fuel treatments.

6. Conclusions and Implications

Conclusions

Across a representative gradient of Alaskan boreal ecosystems and under operationally realistic practices, hand-built pile burns produced a localized, largely downward heat pulse

whose magnitude, duration, and penetration were governed primarily by the thermal state of underlying soils at ignition and by SOL thickness. These controls explain stronger fall heating due to warmer ambient soils, the insulating role of thick organic layers, the limited predictive value of pile size, and the near-term enrichment of plant-available nutrients and pH consistent with an ash-bed effect. Belowground C responses hinged on SOL depth thresholds (15 cm for C), with shallow SOL sites gaining C from ash and charcoal and deeper SOL sites incurring net C losses due to combustion of organic soil. Nitrogen was consistently lost from the belowground pool, with those losses increasing substantially when the depth of the SOL was greater than 25cm. Framed together, timing, placement along SOL gradients, and pile fuel assembly constitute actionable levers for designing prescriptions that meet fuel reduction objectives, modulate disturbance to soil biota and nutrients, and when appropriate use the ash pulse window to help shape vegetation recovery within fuel breaks.

Implications for management

Hand thinned fuel treatments with pile burning are increasingly used in Interior Alaska to reduce wildfire risk while prioritizing ecosystem services and aesthetics. In our study, pile burning produced modest and spatially limited soil effects. Extreme temperatures were uncommon and, when present, were limited to the upper 10 cm of mineral soil beneath the pile footprint. Heating moved downward with no detectable lateral spread. We observed no fire escape or creep beyond pile edges, and burns conducted with at least 3 cm (about 1 inch) of snow cover posed little to no risk of uncontrolled spread. In short, direct soil impacts were small in extent and depth, with nuances that practitioners can manipulate to meet fuel treatment objectives.

Throughout this section, we use “levers” to mean the aspects of implementation that practitioners can actively set to shape outcomes. We investigated three levers in particular: the season when piles are burned, the thickness of the SOL where piles are constructed, and pile volume. Season is the first and most binary lever for soil heating and associated C and N losses from the SOL. In spring, when soils are frozen, heating first drives thaw and phase change of soil water from solid ice to liquid water. This effect (Outcalt et al., 1990) increases the energy required to raise temperature, so a substantial portion of heat is absorbed with little increase in measured soil temperature. As a result, spring burns tended to produce shallower heating and shallower SOL burn depths. Fall burns began over warmer, thawed soils, which allowed heat to translate more efficiently into temperature increases and deeper, though still moderate, penetration. Where minimizing soil disturbance and nutrient loss is the priority, spring conditions are generally favorable. Where slightly greater heating is desired for fuel objectives, fall conditions can be appropriate with awareness of the tradeoff.

Selecting the SOL depth where piles are constructed is the second lever. Soil organic layers deeper than 25cm insulated mineral soils from heating and tended to experience only partial combustion, while thin organic layers allowed heating to reach mineral soil more readily and were more likely to combust fully. We found deeper SOL depths kept the depth where maximum temperature reached 50°C close to the surface and reduced the likelihood of crossing higher biological or chemical thresholds. In contrast, shallow SOL depths (less than 15cm) increased the chance of surpassing these thresholds in the first 30cm of mineral soil. Practically, site selection within a fuel treatment area impacts the amount of heat soils will receive. Constructing piles on sites with moderate to deep SOL depths (15 to 30cm) can reduce soil

heating and C and N loss, while shallow SOL depths call for tighter prescriptions if protection of soil microbes and plants from exposure to high soil temperatures for extended durations is a priority.

The third lever is pile composition. A common belief is that larger piles cause greater soil heating, yet our results and prior research do not support that assumption. Pile volume was a weak predictor, whereas composition mattered more (Busse et al., 2013). Given this finding, we conducted a secondary analysis and found that piles with a higher proportion of large diameter stem or bole pieces tended to prolong flaming and smoldering, increasing the duration soils are exposed to temperatures above 25°C. In practice, composition is a more useful and tunable parameter than volume. To minimize heating, favor smaller fuels such as foliage and branches and stems less than 7.6 cm (3 in) and distribute heavy fuels across many piles to promote fast, efficient combustion with short residence near the soil surface (Brown, 1974). If the treatment objective requires greater heating and SOL combustion within the footprint, increasing the proportion of large pieces per pile can achieve that outcome while staying within burn safety constraints.

These patterns help interpret common fuel treatment scenarios. Where practitioners aim to maintain current stand structure and protect soils with moderate SOL depth, the combination of spring burning, snow cover, and smaller fuels will produce shallower heating and impacts to C and N minimal. Where practitioners aim to encourage a shift in stand composition on sites with shallow to moderate SOL depth, fall burning and a somewhat higher fraction of large diameter material can increase near surface heating and combustion depth in a controlled footprint. Caution should be taken when burning large piles over especially large SOL depths (greater than 35cm) to avoid large losses in C and N within the pile scars. In all cases, an immediately available pulse of soil nutrients from ash presents an opportunity to guide plant regeneration in pile burns with seeding or planting desirable species.

Across scenarios, we suggest the most defensible strategy is to match prescriptions to site sensitivity and goals. Use season to set the overall heating potential. Use SOL depth to guide where piles are placed or whether additional caution is warranted. Use pile composition, more than volume, to fine tune residence time at the soil surface. When these levers are aligned with objectives, pile burning can reduce fuels with minimal and predictable soil effects while supporting timely recovery of soil biota and vegetation.

Implications for future research

An important limitation of this study was our inability to collect volumetric soil moisture content. Further investigations should endeavor to include soil moisture content (both when liquid water and ice) at the time of pile combustion to further quantify the drivers of soil heating in boreal forest soils. This addition would aid in soil heating modeling or predictive efforts and potentially represent an additional practitioner lever to shape soil heating and soil impacts of pile burning.

Pile burning is a widely used and adaptable fire management activity and efforts should be made to measure soil heating and other direct fire effects at the extremes of realistic application (i.e. very large piles, high pile density, saturated soils). Our conclusions do not extend beyond the sampled range of pile volumes, construction types, and landscape characteristics.

Soil amelioration techniques present a simple and potentially important method to encourage and guide soil recovery processes after pile burning (Korb et. al., 2004). In boreal forest soils, we suggest that experimentation with living soil amendments (including both microbes and plants) has potential to aid in recolonization of bacteria and fungi which may have been killed during the pile burn. In areas where colonization of undesirable ruderal or invasive plant species is a concern, this may be a particularly powerful technique and warrants explicit investigation.

Finally, long-term monitoring of burned piles presents an intriguing opportunity to follow soil recovery and organismal regeneration trajectories, including changes to soil temperature, microbial communities and biomass, C and N losses or sequestration, and permafrost thaw where applicable. Linking practitioner levers to long-term recovery processes would further guide recommendations and improve the quality of manager decision making.

Literature Cited

Alexander, H. D., & Mack, M. C. (2016). A Canopy Shift in Interior Alaskan Boreal Forests: Consequences for Above- and Belowground Carbon and Nitrogen Pools during Post-fire Succession. *Ecosystems*, *19*(1), 98–114. https://doi.org/10.1007/s10021-015-9920-7

Antal, M. J., & Grønli, M. (2003). The Art, Science, and Technology of Charcoal Production. *Industrial & Engineering Chemistry Research*, *42*(8), 1619–1640. https://doi.org/10.1021/ie0207919

Bonanza Creek Long-Term Ecological Research Program Climate Database. 2025. Bonanza Creek LTER - University of Alaska Fairbanks (http://www.lter.uaf.edu). National Science Foundation Grant (DEB-2224776 and DEB-1636476) and by the USDA Forest Service, Pacific Northwest Research Station (RJVA-PNW-20-JV-11261932-018).

Brady, M. K., Dickinson, M. B., Miesel, J. R., Wonkka, C. L., Kavanagh, K. L., Lodge, A. G., et al. (2022). Soil Heating in Fire (SheFire): A model and measurement method for estimating soil heating and effects during wildland fires. *Ecological Applications*, *32*(6), e2627. https://doi.org/10.1002/eap.2627

Brooks, M., E., Kristensen, K., Benthem, K., J. ,van, Magnusson, A., Berg, C., W., Nielsen, A., et al. (2017). glmmTMB Balances Speed and Flexibility Among Packages for Zero-inflated Generalized Linear Mixed Modeling. *The R Journal*, *9*(2), 378. https://doi.org/10.32614/RJ-2017-066

Brown, J. K. (1974). *Reducing Fire Potential in Lodgepole Pine by Increasing Timber Utilization*. U.S. Department of Agriculture, Forest Service, Intermountain Forest & Range Experiment Station.

Busse, M. D., Shestak, C. J., & Hubbert, K. R. (2013). Soil heating during burning of forest slash piles and wood piles. *International Journal of Wildland Fire*, *22*(6), 786. https://doi.org/10.1071/WF12179

Clark, M. H., & Duffy, M. S. (2006). *Soil Survey of Denali National Park Area, Alaska*. Fairbanks, AK: USDA NRCS.

Creech, M. N., Katherine Kirkman, L., & Morris, L. A. (2012). Alteration and Recovery of Slash Pile Burn Sites in the Restoration of a Fire-Maintained Ecosystem. *Restoration Ecology*, *20*(4), 505–516. https://doi.org/10.1111/j.1526-100X.2011.00780.x

DeBano, L. F. (1998). *Fire's effects on ecosystems*. New York: J. Wiley.

Duffy, P. A., Walsh, J. E., Graham, J. M., Mann, D. H., & Rupp, T. S. (2005). Impacts of Large-Scale Atmospheric–Ocean Variability on Alaskan Fire Season Severity. *Ecological Applications*, *15*(4), 1317–1330. https://doi.org/10.1890/04-0739

Finkral, A. J., Evans, A. M., Sorensen, C. D., & Affleck, D. L. R. (2012). Estimating consumption and remaining carbon in burned slash piles. *Canadian Journal of Forest Research*, *42*(9), 1744–1749. https://doi.org/10.1139/x2012-112

Fox, J., Weisberg, S., & Price, B. (2025). car: Companion to Applied Regression [Data set]. https://doi.org/10.32614/CRAN.package.car

Hartig, F., Lohse, L., & leite, M. de S. (2024, October 18). DHARMa: Residual Diagnostics for Hierarchical (Multi-Level / Mixed) Regression Models (Version 0.4.7). Retrieved from https://cran.r-project.org/web/packages/DHARMa/index.html

Hinkel, K. M., & Outcalt, S. I. (1994). Identification of heat-transfer processes during soil cooling, freezing, and thaw in central alaska. *Permafrost and Periglacial Processes*, *5*(4), 217–235. https://doi.org/10.1002/ppp.3430050403

Hungerford, R., Harrington, M., William, F., & Gerald, N. (1991). *Proceedings, Management and Productivity of Western-montane Forest Soils: Boise, ID, April 10-12, 1990*. U.S. Department of Agriculture, Forest Service, Intermountain Research Station.

Johnson, B. G., Johnson, D. W., Miller, W. W., Carroll-Moore, E. M., & Board, D. I. (2011). The Effects of Slash Pile Burning on Soil and Water Macronutrients. *Soil Science*, *176*(8), 413. https://doi.org/10.1097/SS.0b013e318223cfad

Johnstone, J. F., Chapin, F. S., Hollingsworth, T. N., Mack, M. C., Romanovsky, V., & Turetsky, M. (2010). Fire, climate change, and forest resilience in interior Alaska. *Canadian Journal of Forest Research*, *40*(7), 1302–1312. https://doi.org/10.1139/X10-061

Jorgenson, M. T., Romanovsky, V., Harden, J., Shur, Y., O'Donnell, J., Schuur, E. A. G., et al. (2010). Resilience and vulnerability of permafrost to climate changeThis article is one of a selection of papers from The Dynamics of Change in Alaska's Boreal Forests: Resilience and Vulnerability in Response to Climate Warming. *Canadian Journal of Forest Research*, *40*(7), 1219–1236. https://doi.org/10.1139/X10-060

Kasischke, E. S., Verbyla, D. L., Rupp, T. S., McGuire, A. D., Murphy, K. A., Jandt, R., et al. (2010). Alaska's changing fire regime — implications for the vulnerability of its boreal forestsThis article is one of a selection of papers from The Dynamics of Change in Alaska's Boreal Forests: Resilience and Vulnerability in Response to Climate Warming. *Canadian Journal of Forest Research*, *40*(7), 1313–1324. https://doi.org/10.1139/X10-098

Knoepp, J. D., DeBano, L. F., & Neary, D. G. (2005). Chapter 3: Soil Chemistry, *4*.

Lamlom, S. H., & Savidge, R. A. (2003). A reassessment of carbon content in wood: variation within and between 41 North American species. *Biomass and Bioenergy*, *25*(4), 381–388. https://doi.org/10.1016/S0961-9534(03)00033-3

Liang, X., Liu, D., Wang, Z., & Wang, J. (2022). Characterizing the dynamics of wildland-urban interface and the potential impacts on fire activity in Alaska from 2000 to 2010. *Landscape and Urban Planning*, *228*, 104553. https://doi.org/10.1016/j.landurbplan.2022.104553

Korb, J. E., Johnson, N. C., & Covington, W. W. (2004). Slash Pile Burning Effects on Soil Biotic and Chemical Properties and Plant Establishment: Recommendations for Amelioration. *Restoration Ecology*, *12*(1), 52–62. https://doi.org/10.1111/j.1061-2971.2004.00304.x

Mack, M. C., Walker, X. J., Johnstone, J. F., Alexander, H. D., Melvin, A. M., Jean, M., & Miller, S. N. (2021). Carbon loss from boreal forest wildfires offset by increased dominance of deciduous trees. *Science*, *372*(6539), 280–283. https://doi.org/10.1126/science.abf3903

Massman, W. J., Frank, J. M., & Mooney, S. J. (2010). Advancing Investigation and Physical Modeling of First-Order Fire Effects on Soils. *Fire Ecology*, *6*(1), 36–54. https://doi.org/10.4996/fireecology.0601036

Miyanishi, K., & Johnson, E. A. (2002). Process and patterns of duff consumption in the mixedwood boreal forest. *Canadian Journal of Forest Research*, *32*(7), 1285–1295. https://doi.org/10.1139/x02-051

Moore, W. E. (1961). *A Method of Charcoal Analysis*. Forest Products Laboratory.

Mott, C. M., Hofstetter, R. W., & Antoninka, A. J. (2021). Post-harvest slash burning in coniferous forests in North America: A review of ecological impacts. *Forest Ecology and Management*, *493*, 119251. https://doi.org/10.1016/j.foreco.2021.119251

National Park Service. (2022). Weather and Climate - Denali National Park & Preserve (U.S. National Park Service). Retrieved January 17, 2024, from https://www.nps.gov/dena/learn/nature/climate.htm

O'Donnell, J. A., Romanovsky, V. E., Harden, J. W., & McGuire, A. D. (2009). The Effect of Moisture Content on the Thermal Conductivity of Moss and Organic Soil Horizons From Black Spruce Ecosystems in Interior Alaska. *Soil Science*, *174*(12), 646. https://doi.org/10.1097/SS.0b013e3181c4a7f8

Ott R.A. & Jandt R. (2005). Fuels Treatment Demonstration Sites in the Boreal. Joint Fire Science Program report.

Outcalt, S. I., Nelson, F. E., & Hinkel, K. M. (1990). The zero-curtain effect: Heat and mass transfer across an isothermal region in freezing soil. *Water Resources Research*, *26*(7), 1509–1516. https://doi.org/10.1029/WR026i007p01509

Pereira, P., Jordán, A., Cerdà, A., & Martin, D. (2015). Editorial: The role of ash in fire-affected ecosystems. *CATENA*, *135*, 337–339. https://doi.org/10.1016/j.catena.2014.11.016

Pingree, M. R. A., & Kobziar, L. N. (2019). The myth of the biological threshold: A review of biological responses to soil heating associated with wildland fire. *Forest Ecology and Management*, *432*, 1022–1029. https://doi.org/10.1016/j.foreco.2018.10.032

Roland, C. A., Schmidt, J. H., & Nicklen, E. F. (2013). Landscape-scale patterns in tree occupancy and abundance in subarctic Alaska. *Ecological Monographs*, *83*(1), 19–48. https://doi.org/10.1890/11-2136.1

Ryan, K. C., Jones, A. T., Koerner, C. L., & Lee, K. M. (2012). *Wildland fire in ecosystems: effects of fire on cultural resources and archaeology* (No. RMRS-GTR-42) (p. RMRS-GTR-42). Ft. Collins, CO: U.S. Department of Agriculture, Forest Service, Rocky Mountain Research Station. https://doi.org/10.2737/RMRS-GTR-42

Santín, C., Doerr, S. H., Merino, A., Bryant, R., & Loader, N. J. (2016). Forest floor chemical transformations in a boreal forest fire and their correlations with temperature and heating duration. *Geoderma*, *264*, 71–80. https://doi.org/10.1016/j.geoderma.2015.09.021

Sayakoummane, V., & Ussawarujikulchai, A. (2009). Comparison of the physical and chemical properties of briquette and wood charcoal in Khammouane province, Lao PDR. *Environment and Natural Resources Journal*, *7*(1).

Smith, J. E., Cowan, A. D., & Fitzgerald, S. A. (2016). Soil heating during the complete combustion of mega-logs and broadcast burning in central Oregon USA pumice soils. *International Journal of Wildland Fire*, *25*(11), 1202. https://doi.org/10.1071/WF16016

Switzer, J. M., Hope, G. D., Grayston, S. J., & Prescott, C. E. (2012). Changes in soil chemical and biological properties after thinning and prescribed fire for ecosystem restoration in a Rocky Mountain Douglas-fir forest. *Forest Ecology and Management*, *275*, 1–13. https://doi.org/10.1016/j.foreco.2012.02.025

Thorpe, H. C., & Timmer, V. R. (2005). Early growth and nutrient dynamics of planted *Pinus banksiana* seedlings after slash-pile burning on a boreal forest site. *Canadian Journal of Soil Science*, *85*(1), 173–180. https://doi.org/10.4141/S04-011

Timur V. Elzhov, Katharine M. Mullen, Andrej-Nikolai Spiess, Ben Bolker. (2022). minpack.lm: R Interface to the Levenberg-Marquardt Nonlinear Least-Squares Algorithm Found in MINPACK, Plus Support for Bounds [Data set]. https://doi.org/10.32614/CRAN.package.minpack.lm

Wang, L., Skreiberg, Ø., Van Wesenbeeck, S., Grønli, M., & Antal, M. J. (2016). Experimental Study on Charcoal Production from Woody Biomass. *Energy & Fuels*, *30*(10), 7994–8008. https://doi.org/10.1021/acs.energyfuels.6b01039

Zuur, A. F., Ieno, E. N., Walker, N., Saveliev, A. A., & Smith, G. M. (2009). *Mixed effects models and extensions in ecology with R*. New York, NY: Springer. https://doi.org/10.1007/978-0-387-87458-6

Appendix A. Contact Information

Michelle Mack, Center for Ecosystem Science and Society, Northern Arizona University, Flagstaff, AZ 86001, USA. Michelle.Mack@nau.edu.

Matt Behrens, Center for Ecosystem Science and Society, Northern Arizona University, Flagstaff, AZ 86001, USA. mcb566@nau.edu.

Appendix B. List of Science Delivery Products

1. Publications

   Thesis for Master of Science student Matt Behrens. Accepted and submitted to Northern Arizona University, December 2025.

   In preparation: *Fire's Footprint: Understanding Soil Heating and Fire Effects in Denali National Park & Preserve's Prescribed Pile Burns* to be submitted for publication in peer-reviewed journal (Fire Ecology). Expected submission February 2026.

2. Knowledge Transfer

   Alaska Interagency Fuels Management Workshop invited presentation, Feb 2025. *Fire's Footprint: Understanding Soil Heating and Fire Effects in Denali National Park & Preserve's Prescribed Pile Burns*

   Northern Arizona University, Center for Ecosystem Science and Society seminar. January 2025. *Fire's Footprint: Understanding Soil Heating and Fire Effects in Denali National Park & Preserve's Prescribed Pile Burns.*

   Association for Fire Ecology Fire Congress, oral presentation, Dec 2025. *Fire's Footprint: Understanding Soil Heating and Fire Effects in Denali National Park & Preserve's Prescribed Pile Burns*

   Planned: Webinar co-produced by Alaska Fire Science Consortium and NPS Alaska.

3. Outreach Materials

   National Park Service Research Brief: *Pile burning effects on boreal soils.*

Appendix C. Metadata

Archived data include individual pile coordinates, and all metrics and measurements collected from that pile or unburned control location. The metadata consist of a description of the study, experimental design, field methods, lab methods, and data. It includes information on the personnel who collected the data, including a contact person. It describes the structure of the data files, each variable in the data and each pile site.

The data and metadata are in the process of being submitted to the Bonanza Creek Long Term Ecological Research Program (BNZ LTER) data catalog and archived with the Environmental Data Initiative. We will provide the Joint Fire Science Program with a DOI when one is available. Data will remain archived at BNZ LTER data portal and co-listed in the Arctic Data Center. Both sites link to the permanent public data archive at the Environmental Data Iniative.

Appendix D. Supplementary Methods

Soil temperature instrumentation

We constructed the iStakes from 0.5 mm-thick red oak, chosen because its thermal conductivity closely resembles that of field-moist soils. Compared to metals or plastics, wood better mimics soil thermal properties and wetting/drying behavior. Each iStake measured 3.3 × 0.5 × 32 cm. We positioned the uppermost iButton (corresponding to 5 cm soil depth) 3 cm from the stake top so that, once buried, no wood was exposed at the soil surface.

We drilled four holes for iButtons using a 5/8″ bit and finished them by hand with a rotary bit to ensure a snug fit. We drilled a 2 mm hole into an upper corner of each iStake to thread 40 cm of 20 ga steel wire, which we attached to a 5 × 30 cm strip of fire shelter material serving as a retrieval flag.

We used unmodified Thermochron iButtons (model DS1921G). Following Roznik and Alford (2012), we waterproofed each iButton against liquid water and vapor. After cleaning and launching the iButtons, we applied a plastic sealant (Plasti Dip) to the seam where the button halves join. We first sprayed the sealant onto a palette and then brushed it onto each iButton. We applied at least three coats to ensure a watertight seal and enough thickness to allow easy removal by hand after deployment.

To install iStakes in frozen, rocky, or very fine soils, we used a pilot hole driver to create insertion holes of exact size without damaging the wood stakes. We fabricated the tool from tool-grade steel and designed it to be driven by hand with a 6.5 kg T-post driver. It consisted of two parts: a removable stake (3.81 cm wide, 34 cm long, 0.635 cm thick), sharpened to a point and welded to an 11.5 cm diameter plate; and a steel pipe handle (101 cm long, 3.82 cm diameter) capped at the top and welded to a matching plate at the bottom. We bolted the stake and handle together at the plate junction, forming a removable and replaceable platform for driving pilot holes in very hard or frozen soils.

Each assembly used four Type-K thermocouple probes (Inconel 600 sheathed, MgO insulated, OD = 0.062″, miniplug termination): two of 100″ length and two of 177″ length. To simplify field use, we fabricated four short Type-K connectors (15 cm, male/female miniplug) and threaded them through waterproof ports in each datalogger case. These flexible connectors allowed probes to be plugged/unplugged without opening the case, protecting the datalogger from moisture and contamination. We recorded data using HOBO 4-channel thermocouple dataloggers (model UX120-014M).

We partially deconstructed selected piles to expose soil at the pile center. We dug a 3 m trench by hand to remove organic soil and reach the mineral surface. At the pile center, we drove the pilot hole to 35 cm depth using the T-post driver. We then removed the tool vertically by hand or with a manual winch attached to a two-ton tripod crane. We gently inserted the iStake until its top iButton sat 5 cm below the mineral soil surface, and we backfilled the resulting 2cm hole with mineral soil.

Temperature time series extension model

We standardized all sensor time series to a common duration of 5,200 minutes at a 3-minute logging interval. For each pile and sensor, records were ordered by elapsed time. When a

series ended before 5,200 minutes, we used the terminal 300 observations to fit an exponential cooling model and extended the series to 5,200 minutes at the same 3-minute interval.

The model was $\text{Temp} = T_\infty + (T_0 - T_\infty) \times e^{-k \times \text{elapsed}}$. In this parameterization, $T_\infty$is the baseline soil temperature expected after full cooling, T_0 sets the amplitude of the decay, and k controls the cooling rate (larger k implies faster decay). We estimated parameters by nonlinear least squares using nlsLM from the minpack.lm package (Timur et al., 2022). Starting values were T_∞= -1°C, T_0 equal to the maximum temperature in the terminal segment, and $k = 0.005$ min-1. These choices constrained unrealistic solutions, promoted monotonic cooling over the tail, and kept the asymptote near observed post-burn conditions.

Soil heating matrices

We converted each pile's raw temperature depth profile into a depth–time temperature matrix. Timestamps were converted to elapsed minutes from the first record; data were then split by timestamp (time slices). For each slice we fit a natural cubic spline across depth using base R, predicting temperature on a regular grid from 0 to 30 cm depths at 0.1 cm resolution. Predicted values were forced to equal the original observations at their measured depths (i.e., we overwrite the spline at observed depths to preserve raw data), and temperatures were lower bounded at −5°C to avoid unrealistic extrapolation.

Pile biomass calibration

To model the relationship between pile dimensions, pile volume, and pile C mass, we deconstructed eleven randomly selected piles not selected for the main experiment from the six sites. We used a custom fabricated sling to lift and weigh the pile piecewise in the field. The sling consisted of two 5′ galvanized steel pipes with heavy canvas stretched between, forming a 5′ × 5′ square with rigid sides. We attached four pulleys to each pipe and threaded ropes through them to cinch the sling and contents. We used a hand winch with an in-line digital scale, anchored to a purpose-built tripod, to lift the sling off the ground. We built the tripod from three 8′ galvanized steel poles (2″ diameter) joined at a cast steel anchor loop rated for 2 tons lifting capacity.

Statistical methods are described in the main methods. Our model produced an adjusted $R^2 = 0.9702$ ($p < 0.001$), and final equation: Dry biomass (kg) = 58.939 × pile volume (m^3) – 17.767.

Carbon and nitrogen accumulation model

We estimated depth-integrated SOL C and N pools from increment-level measurements of bulk density, %C, and %N (see main methods). For each SOL monolith, we computed increment pools (kg element m^{-2}) and formed cumulative depth profiles by summing from the surface downward. For each site (n = 6) and element, we modeled the cumulative pool using a generalized linear model with Gamma error distribution and log link and fixed effect of depth and site. We assessed model adequacy with the DHARMa package and then applied the fitted, site-specific equations to each pile to estimate the C and N pools from the pre- and post-burn SOL depth measurements. We report model parameters and fit in Supplementary Table 3.

Pile composition predictive model

To test the effect of pile composition on soil heating, we selected the duration above 25°C as it is more sensitive to smaller magnitude increases in soil temperature. We screened all

predictors for collinearity using variance inflation factors (VIF < 5; car; Fox et al., 2025) and confirmed non-collinearity. We tested a predictive GLMM framework in which baseline soil temperature, sensor depth, pre-fire SOL depth, pile volume, and large wood volume proportion were fixed effects, and pile within site was a random intercept. Model family and link was chosen to match response scale and distributional shape, guided by residual plots. Diagnostics (DHARMa; Hartig et al., 2024) indicated improved fit of residuals when zero-inflation was included. We compared the full model (with all interactions) to reduced models using AIC and favored the simpler model when ΔAIC > 2, treating ΔAIC < 2 as equivalent support; unsupported interactions were removed and the model refit with main effects only (Zuur et al., 2009). After model reduction, we verified assumptions using simulated residuals via DHARMa and summarized fixed effects with estimates, standard errors, and Wald p-values. Post hoc comparisons used estimated marginal means (emmeans; Lenth et al., 2025) with a Tukey adjustment. To visualize model results, we plotted conditional predictions from the final model holding covariates at their means and sensor depth at 15cm.

Appendix E. Supplementary Data

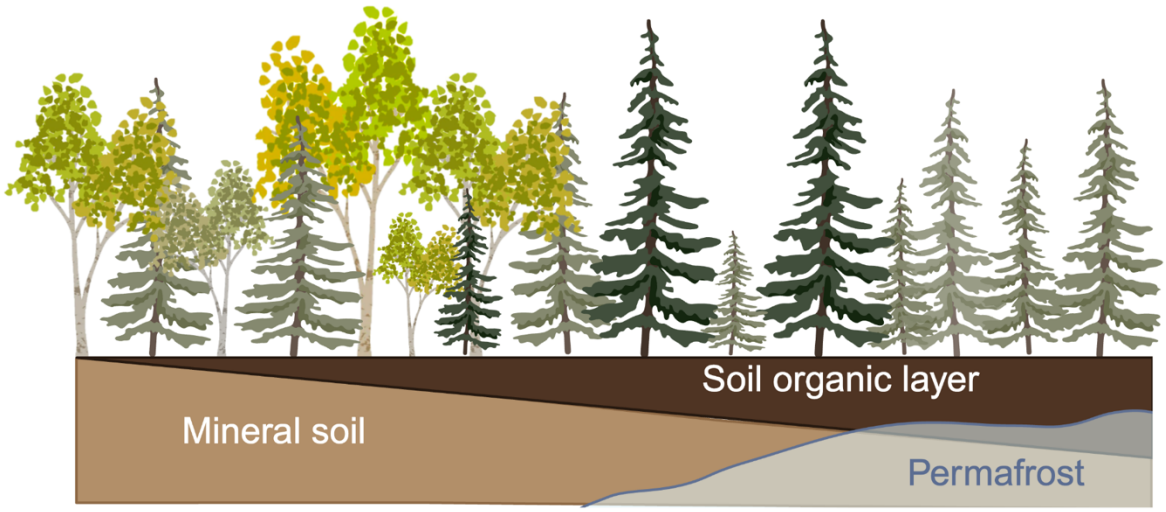

Supplementary Figure 1. Conceptual diagram of forest stand composition, soil organic layer depth, and permafrost presence across study sites.

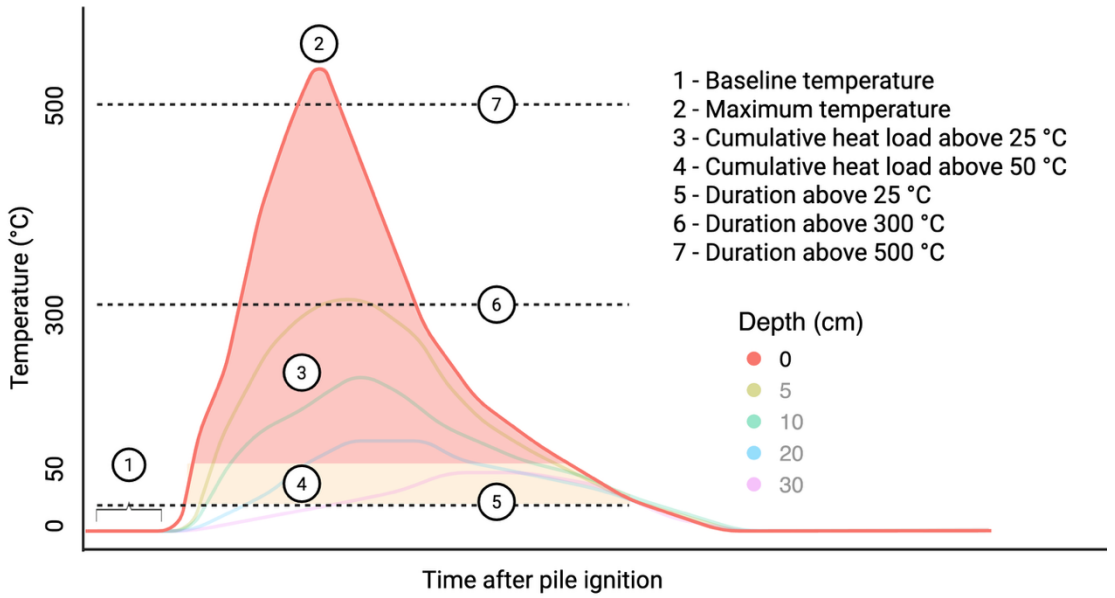

Supplementary Figure 2. Conceptual diagram of a vertical soil heating profile with soil heating metrics displayed.

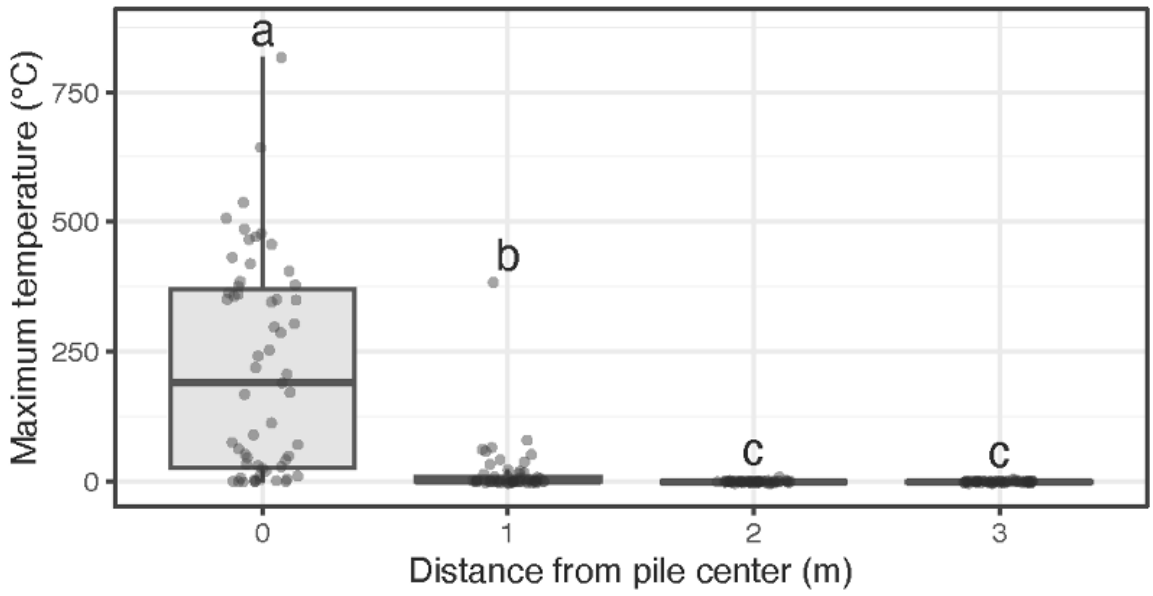

Supplementary Figure 3. Horizontal transect of soil heating at the mineral soil surface (n = 59 for each distance from pile center). Maximum temperature is unmodified from observed data. Mean pile radius was 1.15 (± 0.02) meters. Different letters indicate significant differences among groups ($F_{3, 232}$ =118.1, $p<0.01$).

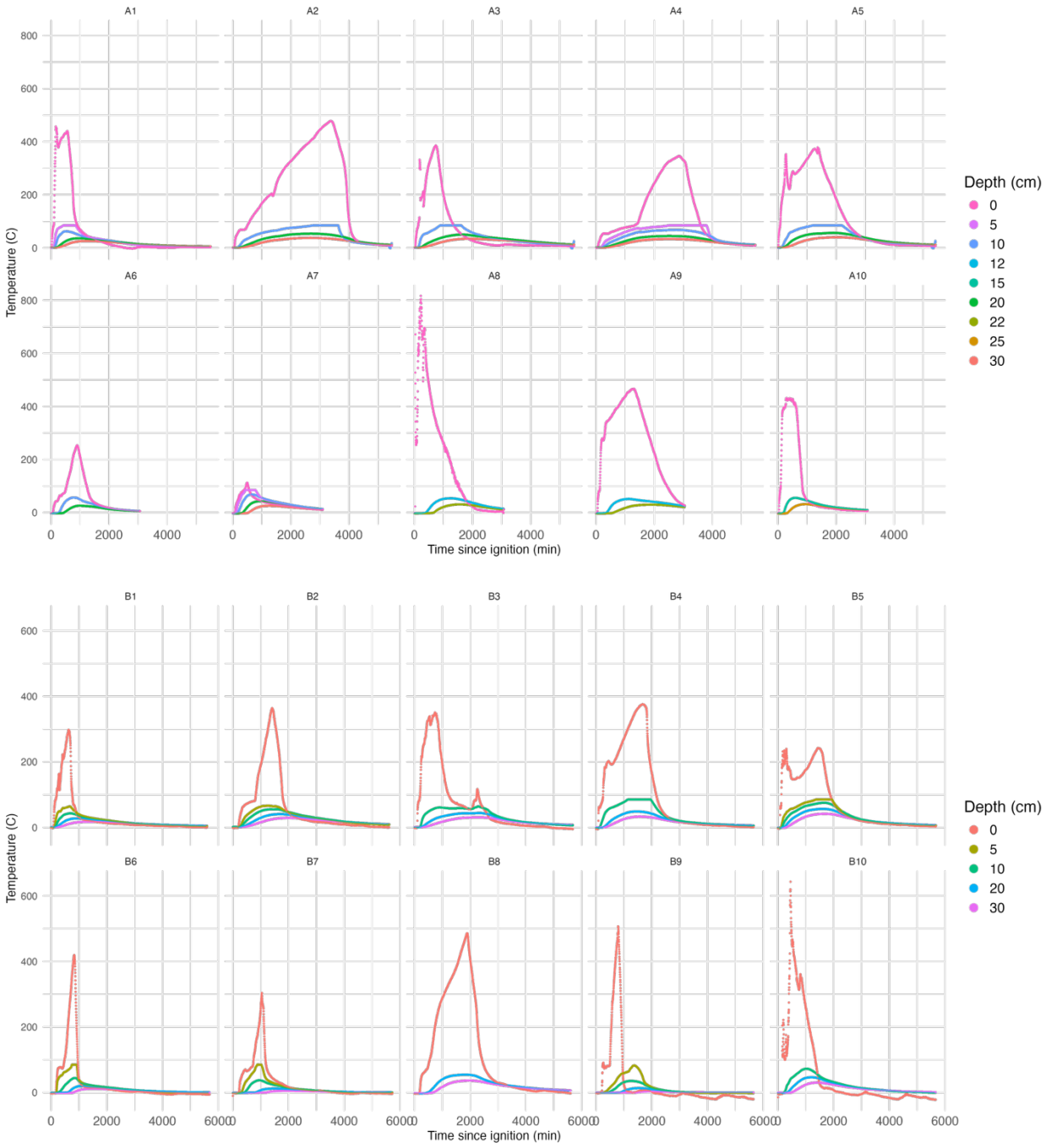

Supplementary Figure 4. Vertical soil heating profiles of individual piles within site A and B. Plots labeled 1-5 were burned in fall 2024, plots labeled 6-10 were burned in spring 2024 for site A and spring 2025 for site B. Where sensor depths are non-standard or missing, sensors were unable to be located at standard depth due to rocky soils or sensors were burned and lost. Data are unmodified from raw sensor records.

Supplementary Figure 5. Vertical soil heating profiles of individual piles within site C and D. Plots labeled 1-5 were burned in fall 2024, plots labeled 6-10 were burned in spring 2025. Where sensor depths are missing, sensors were burned and lost. One pile in site D was burned prior to instrumentation and soil heating data were not collected. Data are unmodified from raw sensor records.

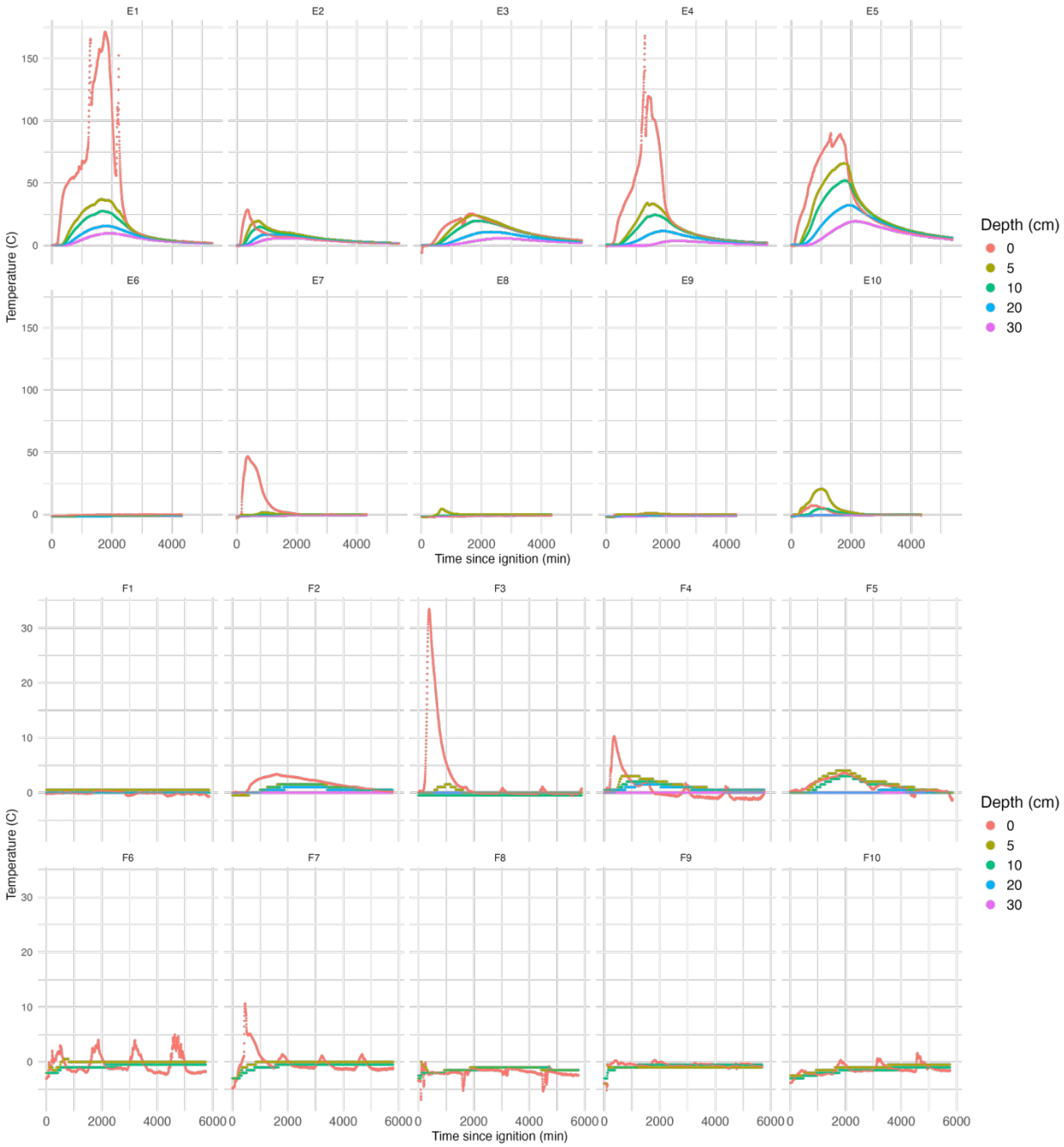

Supplementary Figure 6. Vertical soil heating profiles of individual piles within site E and F. Plots labeled 1-5 were burned in fall 2024, plots labeled 6-10 were burned in spring 2024 for site E and spring 2025 for site F. Where sensor depths are missing, sensors were burned and lost. Data are unmodified from raw sensor records.

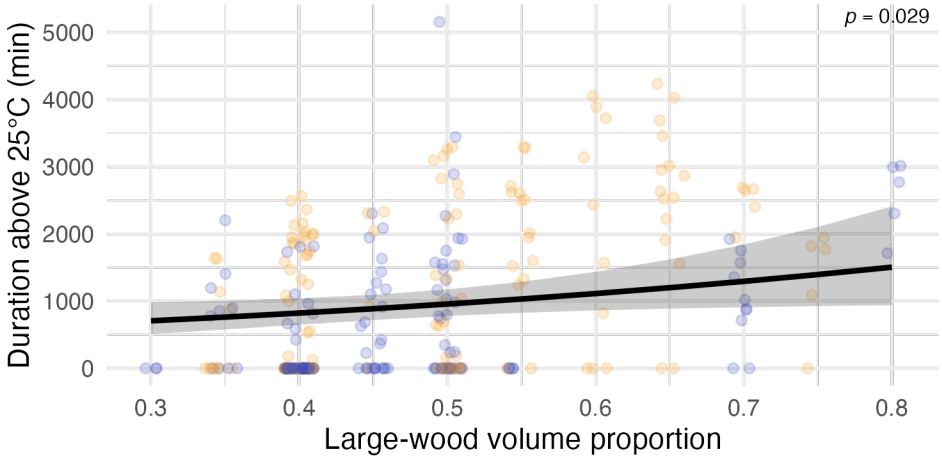

Supplementary Figure 7. Relationship between large-wood volume proportion of pile and the duration above 25°C (minutes) during pile burns. Figure summarize a generalized linear mixed model (GLMM) fit to sensor level data (N = 285). Black line (with 95% CI ribbon) is a GLMM prediction with other covariates held at their sample means and sensor depth fixed at 15 cm; jitter added to points for increased readability; p-values are printed.

Supplementary Table 1. Model results for carbon and nitrogen accumulation.

Site	Nutrient	Intercept	Intercept SE	Slope	Slope SE	t Value	Pr(>|t|)	Maximum depth (cm)
A	C	-0.67021	0.13424	0.10972	0.00559	-4.99	< 0.001	20
	N	2.49768	0.15791	0.12986	0.00679	15.82	< 0.001	
B	C	-1.02838	0.13815	0.10972	0.00559	-7.44	< 0.001	20
	N	2.17045	0.16244	0.12986	0.00679	13.36	< 0.001	
C	C	-0.86893	0.12922	0.10972	0.00559	-6.72	< 0.001	25
	N	2.18000	0.11525	0.12986	0.00679	14.29	< 0.001	
D	C	-0.50239	0.12736	0.10972	0.00559	-3.94	< 0.001	30
	N	2.79512	0.15100	0.12986	0.00679	18.51	< 0.001	
E	C	1.08988	0.12997	0.10972	0.00559	-8.38	< 0.001	35
	N	1.89389	0.15512	0.12986	0.00679	12.21	< 0.001	
F	C	-0.63889	0.13134	0.10972	0.00559	-4.86	< 0.001	40
	N	2.55907	0.15378	0.12986	0.00679	16.64	< 0.001	

Supplementary Table 2. Charcoal percent carbon literature review reference values.

Source	Charcoal Type	% Carbon
(Sayakoummane & Ussawarujikulchai, 2009)	Hardwood	69.92
		58.33
		63.24
		73.92
	Softwood	73.24
		61.23
(Wang et al., 2016)	Spruce	94.97
		85.8
		78.6
	Birch	85.39
		92.67
(Moore, 1961)	Hardwood	84.65
		83.56
		84.9
		81.61
		82.22
		78.24
		77.9
		70.68
(Antal & Grønli, 2003)	Hardwood	69.9
		91.5
	Softwood	92.84
	Birch	94.58
		72.5
		77.2
	Spruce	79.1
		69.1
		74.7
	Pine	78.7
		69.6
		74.6
		78.8
		86.6
(Finkral et al., 2012)	Ponderosa	78.4

Supplementary Table 3. Initial model specifications for soil heating, carbon and nitrogen additions and losses, and burn depth.

Response family	Response	Error Distribution (link)	Predictors	Interactions	Random Effects
Soil heating	MaxT†	Gamma (log)	Season, Pile volume, Pre-fire SOL depth, Sensor depth	Season x Pile volume, Season x Pre-fire SOL depth, Pile volume x Pre-fire SOL depth	Pile within Site
	CHL25	Poisson (log)			
	CHL50	Negative binomial (log)			
	Time25	Truncated neg binomial (log)^			
	Time300	Negative binomial (log)			
	Depth50 (occurrence)	Binomial (logit)	Season, Pile volume, Pre-fire SOL depth	Season x Pile volume, Season x Pre-fire SOL depth, Pile volume x Pre-fire SOL depth	Site
	Depth50 (conditional)	Gamma (log)			
Carbon and Nitrogen addition and loss	Change in belowground C†	Gaussian (identity)			
	Charcoal C addition	Log normal (log) *			
	Ash C addition	Log normal (log)			
	SOL C loss	Log normal (log)			
	Change in belowground N†	Gaussian (identity)			
	Ash N addition	Log normal (log)			
Burn depth	Burn depth	Gaussian (identity)***	Season, Pile volume, Pre-fire SOL depth	Season x Pile volume, Season x Pre-fire SOL depth, Pile volume x Pre-fire SOL depth	Site
Baseline soil temperature	Baseline	Gaussian (identity)	Season	None	Site

† Response a sin h transformed. * Dispersion factor of site. ** Dispersion factor of sensor depth + site. *** Dispersion factor of season. ^ Zero inflation formula of sensor depth

Supplementary Table 4. Estimates, confidence intervals (CI), p-values, and Marginal and Conditional R^2 ($M\text{-}R^2$ and $C\text{-}R^2$) from generalized linear mixed effect models of soil heating responses.

Model	Predictors	Estimate	CI	p-value	ICC	$M\text{-}R^2$ ($C\text{-}R^2$)
Maximum temperature[†]	(Intercept)	2.1	1.42 – 2.79	**<0.001**	0.64	0.326 (0.756)
	Season [Spring]	-0.42	-0.58 – -0.25	**<0.001**		
	Pre-fire SOL depth	-0.01	-0.03 – -0.00	0.159		
	Pile volume	0.02	-0.03 – 0.07	0.369		
	Sensor depth	-0.05	-0.06 – -0.05	**<0.001**		
Duration above 25C[+]	(Intercept)	5436.9	2317.4 – 12755.5	**<0.001**	0.77	0.563 (0.899)
	Season [Spring]	0.55	0.39 – 0.78	**0.001**		
	Pre-fire SOL depth	0.93	0.9 – 0.96	**<0.001**		
	Pile volume	1.04	0.95 – 1.15	0.363		
	Sensor depth	0.98	0.97 – 0.98	**<0.001**		
Duration above 300C[+]	(Intercept)	1430.9	57.4 – 35659.7	**<0.001**	1	0.627 (0.999)
	Season [Spring]	0.37	0.15 – 0.88	**0.025**		
	Pre-fire SOL depth	0.88	0.78 – 1	0.053		
	Pile volume	0.96	0.77 – 1.2	0.749		
Cumulative Heat Load above 25C[+]	(Intercept)	22814.8	2125.7 – 244864.5	**<0.001**	1	0.647 (1.00)
	Season [Spring]	0.41	0.18 – 0.97	**0.043**		
	Pre-fire SOL depth	0.85	0.78 – 0.94	**0.001**		
	Pile volume	1.03	0.82 – 1.3	0.805		
	Sensor depth	0.86	0.86 – 0.87	**<0.001**		
Cumulative Heat Load above 50C[+]	(Intercept)	1061.4	61.8 – 18232	**<0.001**	1	0.547 (1.0)
	Season [Spring]	0.32	0.16 – 0.63	**0.001**		
	Pre-fire SOL depth	0.94	0.86 – 1.02	0.154		
	Pile volume	1.09	0.89 – 1.33	0.396		
	Sensor depth	0.78	0.76 – 0.80	**<0.001**		

Depth to reach 50C						
Occurrence model*	(Intercept)	13591431	85 –2169127365280	**0.007**	0.98	0.036 (0.981)
	Season [Spring]	0.01	0.00 – 0.5	**0.02**		
	Pre-fire SOL depth	0.89	0.68 – 1.16	0.382		
	Pile volume	0.61	0.32 – 1.15	0.128		
Conditional model^	(Intercept)	11.5	3.91 – 33.86	**<0.001**	0.33	0.215 (0.472)
	Season [Spring]	0.68	0.45 – 1.01	0.057		
	Pre-fire SOL depth	0.97	0.92 – 1.01	0.135		
	Pile volume	1.17	1.03 – 1.34	**0.019**		
Baseline soil temperature^	(Intercept)	0.36	0.03 – 0.68	**0.031**	0.11	0.693 (0.727)
	Season [Spring]	-2.24	-2.6 – -1.88	**<0.001**		

Note: Bolded p-values indicate significance (<0.05).

† Transformed estimate (a sin h).

+ Incident rate ratio.

* Odds ratio.

^ Estimate.

Supplementary Table 5. Estimates, confidence intervals (CI), p-values, and Marginal and Conditional R^2 ($M\text{-}R^2$ and $C\text{-}R^2$) from generalized linear mixed effect models of carbon and nitrogen additions and losses.

Model	Predictors	Estimates	CI	p-value	ICC	$M\text{-}R^2$ ($C\text{-}R^2$)
Change in belowground C	(Intercept)	-0.19	-2.72 – 2.34	0.881	0.19	0.397 (0.511)
	Season [Spring]	-0.6	-1.17 – -0.02	**0.042**		
	Pre-fire SOL depth	0.04	-0.07 – 0.15	0.483		
	Pile volume	-0.5	-1.01 – 0.01	0.056		
	Pre-fire SOL depth x Pile volume	0.03	0.00 – 0.05	**0.021**		
SOL burn depth	(Intercept)	2.51	1.86 – 3.17	**< 0.001**	0.004	0.006 (0.010)
	Season [Spring]	-0.28	-0.43 – -0.13	**<0.001**		
	Pre-fire SOL depth	0	-0.02 – 0.03	0.987		
	Pile volume	-0.18	-0.32 – -0.04	**0.011**		
	Pre-fire SOL depth x Pile volume	0.01	0.00 – 0.02	**0.002**		
Charcoal C addition	(Intercept)	-0.49	-1.01 – 0.04	0.068	0.417	0.075 (0.461)
	Season [Spring]	-0.12	-0.28 – 0.05	0.165		
	Pre-fire SOL depth	-0.01	-0.02 – 0.01	0.473		
	Pile volume	-0.06	-0.10 – -0.02	**0.009**		
Ash C addition	(Intercept)	-1.02	-1.48 – -0.55	**<0.001**	0.51	0.006 (0.511)
	Season [Spring]	-0.01	-0.16 – 0.13	0.849		
	Pre-fire SOL depth	0	-0.02 – 0.01	0.816		
	Pile volume	0.01	-0.04 – 0.05	0.785		
SOL C loss	(Intercept)	0.02	-0.54 – 0.57	0.952	0.1	0.054 (0.146)
	Season [Spring]	-0.16	-0.32 – -0.00	**0.049**		
	Pre-fire SOL depth	0.03	0.02 – 0.05	**<0.001**		
	Pile volume	0.02	-0.02 – 0.06	0.371		
Change in belowground N	(Intercept)	0.78	-0.07 – 1.63	0.072	0.48	0.445 (0.713)
	Season [Spring]	0.42	0.16 – 0.67	**0.001**		
	Pre-fire SOL depth	-0.09	-0.12 – -0.06	**<0.001**		
	Pile volume	-0.03	-0.11 – 0.05	0.458		
Ash N addition	(Intercept)	2.50	2.04 – 2.96	**<0.001**	0.00	0.000 (0.001)
	Season [Spring]	-0.01	-0.16 – 0.13	0.849		

	Pre-fire SOL depth	-0.00	-0.02 – 0.01	0.816		
	Pile volume	0.01	-0.04 – 0.05	0.785		

Note: Bolded p-values indicate significance (<0.05).

Supplementary Table 6. Estimates, confidence intervals (CI), p-values, and Marginal and Conditional R^2 (M-R^2 and C-R^2) from generalized linear mixed effect models of univariate nutrient availability.

Model	Predictors	Estimate	CI	p-value	M-R^2 (C-R^2)
ph†	(Intercept)	5.62	5.10 – 6.13	**<0.001**	0.285 (0.366)
	Treatment [Fall]	1.79	1.30 – 2.29	**<0.001**	
	Treatment [Spring]	0.62	0.14 – 0.11	**0.012**	
Ammonium‡	(Intercept)	0.11	0.06 – 0.20	**<0.001**	0.273 (0.471)
	Treatment [Fall]	3.38	2.05 – 5.56	**<0.001**	
	Treatment [Spring]	4.12	2.50 – 6.79	**<0.001**	
Nitrate‡	(Intercept)	0.03	0.02 – 0.06	**<0.001**	0.441 (0.556)
	Treatment [Fall]	5.26	3.14 – 8.81	**<0.001**	
	Treatment [Spring]	7.98	4.70 – 13.54	**<0.001**	
Phosphorus‡	(Intercept)	0.10	0.08 – 0.12	**<0.001**	0.762 (0.769)
	Treatment [Fall]	9.96	7.54 – 13.17	**<0.001**	
	Treatment [Spring]	8.12	6.16 – 10.69	**<0.001**	
Potassium‡	(Intercept)	5.60	3.86 – 8.13	**<0.001**	0.375 (0.459)
	Treatment [Fall]	3.23	2.22 – 4.70	**<0.001**	

	Treatment [Spring]	3.61	2.50 – 5.20	**<0.001**	
Calcium‡	(Intercept)	3.98	2.41 – 6.57	**<0.001**	0.501 (0.720)
	Treatment [Fall]	4.17	3.22 – 5.40	**<0.001**	
	Treatment [Spring]	4.90	3.79 – 6.32	**<0.001**	

Note: Bolded p-values indicate significance (<0.05).

† Gaussian error distribution with identity link.

‡ Gamma error distribution with log link.

Supplementary Table 7. Principal component analysis nutrient loadings.

Nutrient	PC1	PC2
S	0.3363	0.1350
Mg	0.3349	0.1446
Ca	0.3116	0.2500
Mn	0.3068	0.0243
Fe	0.3030	0.1194
Zn	0.3019	0.0476
Cu	0.2919	0.0087
Al	0.2771	0.2459
P	0.2677	0.2395
NO3	0.2512	0.0293
K	0.1190	0.4987
NH4	0.1705	0.4605
Pb	0.1557	0.4144
B	0.1787	0.2619
Cd	0.0636	0.2474

Supplementary Table 8. Estimates, confidence intervals (CI), and p-values from generalized linear mixed effect model of duration above 25°C using predictive framework.

Model	Predictors	Estimates	CI	p-value
Duration above 25C (predictive)†	(Intercept)	1850.29	716.6 – 4777.2	**<0.001**
	Sensor depth	0.98	0.98 – 0.98	**<0.001**
	Baseline soil temperature	1.18	1.06 – 1.32	**0.003**
	Large wood volume proportion	4.53	1.17 – 17.61	**0.029**
	Pre-fire SOL depth	0.95	0.93 – 0.98	**0.001**

Note: See Supplementary Methods for model selection methods and model form. Bolded p-values indicate significance (<0.05).

† Truncated negative binomial error distribution with log link.